MULTISPECTRAL ANALYSIS OF CYANOBACTERIA IN THE IJSSELMEER

YIERI JUSTIN
April, 2016

SUPERVISORS:
Dr. Ir. Mhd. Suhyb Salama
Prof. Dr. Ing Wouter Verhoef

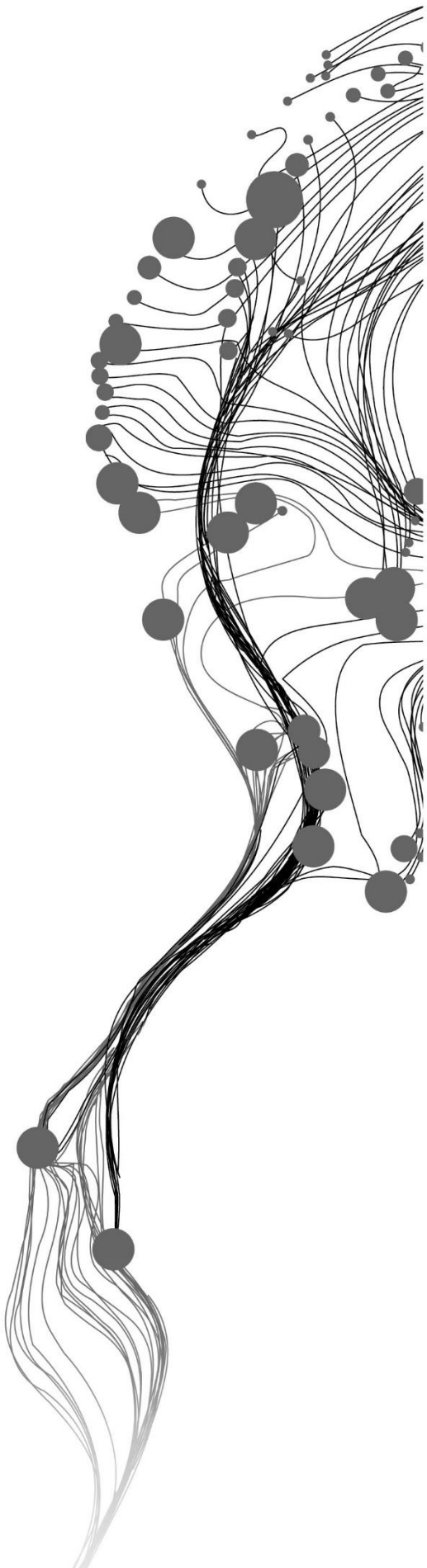

MULTISPECTRAL ANALYSIS OF CYANOBACTERIA IN THE IJSSELMEER

YIERI JUSTIN
Enschede, The Netherlands, April, 2016

Thesis submitted to the Faculty of Geo-Information Science and Earth Observation of the University of Twente in partial fulfilment of the requirements for the degree of Master of Science in Geo-information Science and Earth Observation.
Specialization: Water resources and environmental management

SUPERVISORS:
Dr. Ir. Mhd. Suhyb Salama
Prof. Dr. Ing. Wouter Verhoef

THESIS ASSESSMENT BOARD:

Chair:	Dr. ir. C.M.M. Mannaerts (WRS - ITC)
External:	Dr. A. Vrieling (NRS - ITC)
First Supervisor:	Dr. ir. S. Salama (WRS - ITC)
Second Supervisor:	Prof. Dr. Ing. W. Verhoef (WRS - ITC)

DISCLAIMER

This document describes work undertaken as part of a programme of study at the Faculty of Geo-Information Science and Earth Observation of the University of Twente. All views and opinions expressed therein remain the sole responsibility of the author, and do not necessarily represent those of the Faculty.

ABSTRACT

Climate change and it associated factors has heightened the awareness in the field of biodiversity conservations and the protection of natural resources of which water resources thus inland lakes, rivers, maritime coast land to mention but a few are a part. Protecting and or monitoring the safety of water resources of bacteria has been studied for some time now. The study of these bacteria generally uses traditional methods which involve field visits, measurement and the collection of samples to be tested in the laboratory. These methods are cumbersome and do not cover large spatial areas. The use of satellite remote sensing to help solve these problems has seen tremendous advancement since its introduction. Satellite remote sensing of inland water bodies has improved the monitoring of these resources. The increased use of these remote sensing methods therefore mean the development of new and improve methods of monitoring inland waters.

This research was commissioned in line with this. With the introduction of new and improved sensors, newer models and approaches are needed for monitoring these inland water bodies. This research therefore looks into two semi-empirical models and their ability to derive useful information from sensor images and the ability to use these model for estimating Phycocyanin (PC) in the Ijsselmeer. The two model compared here are the models of Sun et al. and Vincent et al., these models were compared and the best performing model was then adopted for the Ijsselmeer. The models were calibrated and validated with real-time field measurement obtained from the Royal Dutch Ministry of transportation and water management. The model of Sun performed well in prediction the r^2 (0.6993) but was not well in terms of MAPE and RMSE thus 1186.72 % and 9228.06 respectively. Vincent model on the other hand, obtained an r^2 of 0.7163 a MAPE of 18.11 % and RMSE of 646.51.96 for Landsat 8 OLI sensor. When Sentinel-2 MSI was validated the following results were obtained. r^2 of 0.5255, MAPE of 309.88 % and RMSE of 13651.64 for sun model. Vincent model produced the following results, r^2 of 0.0485, MAPE of 21.04 % and RMSE of 866.34.

Based on these results and the fact that Sun model had too many parameters to estimate, the model was dropped whiles Vincent model was used in further processing.

The final results indicated that these was no correlation between the measured PC and that simulated from the sensor.

ACKNOWLEDGEMENTS

I would start my acknowledgement with a quote from Winston Churchill which says "*Success is not final, failure is not fatal: it is the courage to continue that counts*". If I may I will like to add to this by saying, stopping at "success" after a difficult time is a failure.

I would like to extend my gratitude to my supervisor, Dr. Ir. Mhd. Suhyb Salama for the time, support and advice during my research work and the kind monitoring you offered me while supervising this work. Prof. Dr. Ing. Wouter Verhoef my second supervisor I say thank you so much and may the Good lord guide you in your life of retirement.

I would also like to thank the chairman of my department Prof. Dr. Bob Z. Su and the Course director Ir. Arno A. M. van Lieshout for understanding and the support offered me during my difficult times. I will like to thank the administrative secretaries, Mrs Tina E. L. Butt-Castro and Mrs. Anke J. de Koning for your support and kind words as well.

To my fellow colleagues who we brainstormed and discussed issues especially Peter N. Mahama, Nuhu Mujeed and Christian Kwasi Owusu and to the Ghanaian community of ITC, I say thank you so much.

To the Yieri family of Charia in Ghana I say thank you so much for the support, love, care and prayers shown and offered me.

I thank the Lord almighty for seeing me through what was a difficult time. Leaving family and loved once to study abroad. Falling sick and had to be in the hospital without family and loved ones around.

TABLE OF CONTENTS

LIST OF FIGURES

LIST OF TABLES

LIST OF ABBREVIATIONS

Term	Description
Chl-a	Chlorophyll-a
Ed	Downwelling radiance
ENVI	Environment for visualizing image
ESA	European Space Agency
fAPAR	Fraction of absorbed photosynthetically active radiation
FLAASH	Fast Line of Sight Atmospheric Analysis of spectral Hypercubes
LAI	Leaf area index
Lu	Upwelling irradiance
MAE	Mean Absolute Error
MERIS	Medium Resolution Imaging Spectrometer
MSI	Multi-Spectral Instrument
NIR	Near Infrared
NTU	Nephelometric Turbidity Unit
OLI	Operational Land Imager
PC	Phycocyanin
r	Coefficient of correlation
R2	Coefficient of determination
RFU	Relative Fluorescence Unit
RMSE	Root mean square error
Rrs	Remote Sensing reflectance
SNR	Signal to Noise ratio
SRF	Spectral Response Function
SSD	Spatial Sampling Distance
USGS	United State Geological Survey
WHO	World Health Organization
WISP-3	Water Insight Spectrometer

1. INTRODUCTION

For decades, sensors on earth observing satellites have been employed for the synoptic monitoring of phytoplankton in water surface with potential for detecting cyanobacteria (Mishra et al., 2013; Simis et al., 2005). Cyanobacteria contains a characteristic photosynthetic pigment known as phycocyanin (PC) which has a distinctive absorption feature at 620 nm that can be detected using remote sensing techniques and thus a good measure of cyanobacteria (Glazer, 1989; Hunter et al., 2010; Jupp et al., 1994; Richardson, 1996; Ruiz-Verdú et al., 2007; Simis et al., 2005) . It has also been studied that, freshwater cyanobacteria is the main microorganisms that produce relative qualities of PC (Brient et al., 2008) and, therefore, the focus of this MSc thesis work.

The increased occurrence of cyanobacteria in the IJsselmeer is deteriorating its ecosystem services as a result of increased human activities and natural changes (Simis, 2006). Cyanobacteria also referred to as blue-green algae is a unicellular organism that usually occurs in water under favourable conditions (Kudela et al., 2015; Isenstein et al., 2014; Mishra & Mishra, 2014). The necessity for spatial information on cyanobacteria has led to the development of methods and procedures for detecting and quantifying them for better management of inland water (FAO, 2006).

In this thesis, we researched the capability of Landsat 8 operational land imager (OLI) and Sentinel-2 multispectral imager (MSI), hereafter referred to as multispectral instruments in detecting cyanobacteria in the IJsselmeer.

1.1. Problem Statement

Inland water suffers from cyanobacteria bloom which threatens the quality of these water bodies. The thriving of cyanobacteria is sensed optically by measuring the surface concentrations of the Phycocyanin (PC) pigments (Kudela et al., 2015). Some Cyanobacteria produces toxins that are harmful to both human and aquatic life (Cheung et al., 2013) and, therefore, will need to be investigated and controlled especially in inland waters that are used for recreational and fishing purposes (Codd et al., 1999; Dekker, 2004) and in this case, IJsselmeer.

Nevertheless, the detection of cyanobacteria in inland waters using remote sensing is hindered by coarse resolution of current ocean colour satellites (Dekker et al., 1991). MERIS satellite had a spatial resolution of 300 meters and a dedicated 620 nm band for the detection of PC (Reinart & Kutser, 2006; Simis, 2006) and had been used in detecting and estimating PC until April 2012 when it stopped operating.

The recent launch of fine resolution multispectral instruments with a spatial resolution of between 30 and 10 meters for Landsat 8 OLI and Sentinel-2 MSI respectively provides opportunities to map cyanobacteria in inland water bodies at a finer scale. However, there are spectral limitations of the newly launched multispectral instruments. They do not have the 620 nm band for the absorption of suspended sediments (PC) and Signal to Noise Ratio (SNR) is very low.

Below in Table 1-1 are the spectral and temporal characteristics of these multispectral instruments and MERIS.

Table 1-1 Characteristics of Multispectral sensors

Multispectral Sensor characteristics	Landsat 8 OLI	Sentinel-2 MSI	MERIS
Spatial Resolution (meters)	30	10, 20, 60	300
Revisit time (Days)	16	5	3
SWATH Width (Km)	180	290	1150
Spectral bands	9	13	15
Spectral range (nm)	435-1384	443-2190	412-950
Spectral limitations	Lacks the 620 nm wavelength	Lacks the 620 nm wavelength	No spectral limitation, as it was the best sensor for inland water parameters
REFERENCE	usgs, (2013)	ESA, (2015)	(ESA, 2006)

1.2. Research objectives

1.2.1. General Objective

The main objective of this study was to analyse the Multispectral signature of cyanobacteria (PC) for Landsat-8 OLI and Sentinel-2 MSI sensors using the best of Sun et al or Vincent et al models.

1.2.2. Specific objectives

The specific objectives of this research include.

1. To calibrate, validate and compare these existing models for cyanobacteria estimation using in-situ and multispectral data.
2. To investigate the applicability of the best model on these multispectral instruments.

1.3. Research questions

It is important to focus on the scientific applicability of the multispectral instruments with reference to detecting cyanobacteria at a fine scale. Therefore, these questions were to be addressed.

1. Can we deduce useful information from multispectral analysis of cyanobacteria?
2. What is the accuracy of derived cyanobacteria products from Landsat 8 OLI and Sentinel-2 MSI?
3. How do cyanobacteria vary at fine spatial scale?

2. LITERATURE REVIEW

2.1. Cyanobacteria

Blue-green algae is another name for cyanobacteria which is an important class of phytoplankton (Griffiths, 1939; Simis, 2006; Vincent, 2009). The need to know more on cyanobacteria has grown over the years with lots of work done on eutrophic water and slow moving inland water bodies (Ogashawara et al., 2013). The uncontrolled growth of these cyanobacteria threatens life and property (Bartram et al., 1999). This therefore increases the need to look into cyanobacteria.

Several works have been done in this area to help address the problem associated with cyanobacteria growth and impact of both life and property. Researches done in this field are generally grouped into three main categories thus, false Colour Composite-based, index-based and water quality parameters retrieval-based (Zheng Zhou et al., 2011). These approaches are based on analytical algorithms, empirical and semi-empirical algorithms. These models have over the year proved to be useful in the estimating cyanobacteria with some particular satellites like MERIS (Guanter et al., 2010; Medina-Cobo et al., 2014; Ruiz-Verdú et al., 2007). The need to expand the scope of these models is imminent and needed to monitor water bodies in the event of one sensor being rendered non-operational like MERIS since 2012.

2.2. Phycocyanin (PC)

PC is a type of cyanobacteria that is beneficial and at the same time can be harmful. Several methods of monitoring these cyanobacteria have been proposed by many researchers with the use of remote sensing. One of such approaches is the use of chlorophyll a (Gons, 2002) as a proxy for monitoring PC.

According to Kudela et al. (2015), it is a complex protein pigment whiles Vincent et al. (2004) describe it as a pigment specific to cyanobacteria. This pigment absorbs light between the range of 600 and 625 nm with excitation at the same wavelength ranges. It also emits light at around 665 nm (Brient et al., 2008; Dekker, 1993; Reinart & Kutser, 2006). The study of PC has revealed that emitted PC fluorescence is directly proportional to the concentration of PC at any given point (Chawira, 2012). With this assumption, PC fluorescence can be used as a measure of the level of concentration in a water body.

Eutrophication is a major contributing factor to the bloom of PC among other factors which were found in the works of Ahn et al. (2007) and Guanter et al. (2010). In their works, it was observed that PC in the IJsselmeer is dominant in the summer when conditions are favourable for their bloom.

2.2.1. Phycocyanin Measurement

PC measurement and quantification have led to the development of several models(Mishra & Mishra, 2014; Matthews et al., 2012; Simis, 2006; Vincent et al., 2004). In a recent work by Sun et al. (2015) four (4) of the developed models were identified that could be applied on satellite images these include:, multivariate band ratio regression model (Vincent et al., 2004), semi-analytical model (Simis et al., 2005),band ratio quadratic empirical model (Hunter et al., 2010) and spectral slope empirical model (Dash et al., 2011). In 2013 however, Mishra et al. (2013) developed a quasi-analytical approach of quantifying cyanobacteria, which incorporates the working theory of Simis et al. (2005) semi-analytical band ratio model based on apparent and inherent optical properties of water (Gordon et al., 1988; Z. Lee et al., 1994) to retrieve total absorption of PC at 620 nm which is the reference peak of phycocyanin absorption spectrum.

The application of the above-mentioned models is limited, leading from the availability of medium to high-resolution sensors that have the required band (620 nm band) for the application of these models and spatial-

temporal limitations usually associated with these sensors. As a result of this band limitation, some models apply implicit correlation using the absorption and scattering properties of sensors, for instances Landsat sensors (Kutser, 2009). Whiles some also tend to be more practical by taking into consideration the optical variables and water constituents (Vincent et al., 2004). The performances of models however depended basically on the strengths and weaknesses of these models, the spectral band availability and the methodological biases (Ruiz-Verdú et al., 2007).

The study was therefore intended to assess two semi-empirical models (Sun et model and Vincent et al model) based on currently available models and to find out how applicable the nest model would be on Landsat 8 OLI and Sentinel-2 MSI data for the IJsselmeer.

3. STUDY AREA AND DESCRIPTION OF DATA

3.1. STUDY AREA

The study area for this research is IJsselmeer in the Netherlands. It is the largest freshwater lake in the Netherlands described as a shallow eutrophic freshwater lake. It is bordered by the provinces of North Holland, Friesland and Flevoland. The IJsselmeer was originally part of the Zuider Zee sea which was reclaimed in the year 1932 with the construction of a dike (Dekker, 2004; The Columbia Encyclopedia, 6th ed., 2015). Since the construction of the dike, the lake has served as both a source of income and recreation for inhabitants around the lake (TheIJsselmeer.com, 2016).

3.1.1. Location and size

The IJsselmeer is located in the northwestern part of the Netherlands between latitude 52º 49'N and longitude 5º 15' E. In 1976, a dike was constructed on Wadden Sea creating the IJsselmeer and the Markemeer with approximately 1190 km² and 620 km² respectively (Dekker, 2004; Simis et al., 2005). IJsselmeer has a mean depth of approximately 4.4 m, Secchi disk depth of approximately 0.8m (Simis et al., 2005; Simis, 2006).

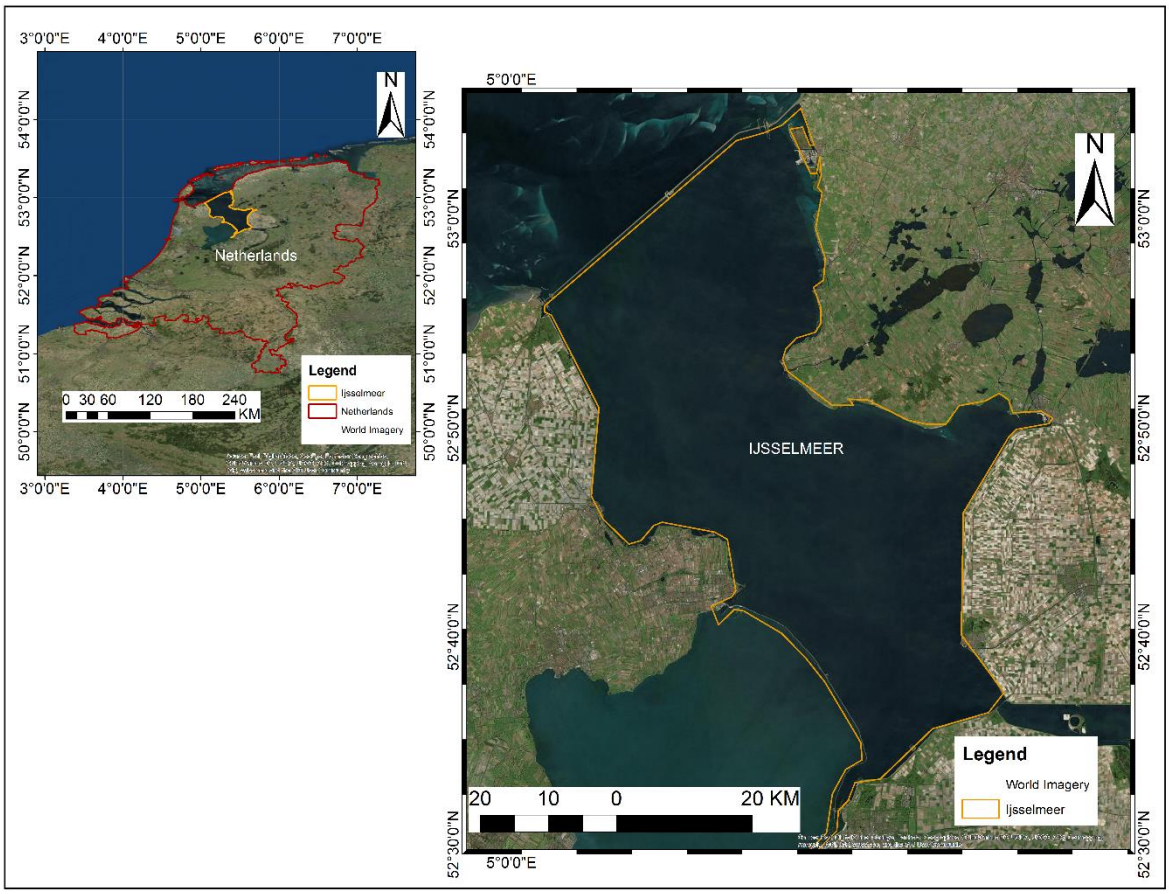

Figure 3-1. Map of the study area overlaid on Google world imagery map. On the left is a context map of the Netherlands on a google world image with the location of the study area. On the right is a layer zoomed to study area.

3.1.2. Geography of the lake

The location of the lake is generally affected by south-western winds resulting in maritime climatic conditions (Lorenz, 1999) . Precipitation in this part of the country is all year round with an almost even distribution amongst all months of the year. For this reason, the IJsselmeer was designed to discharge water into neighbouring lakes and canals during winter to prevent floods and allow in water from neighbouring lake and canals to prevent water shortage in the summer (Lorenz, 1999; Simis et al., 2005; Simis, 2006). The IJsselmeer is drained mainly by the river Rhine.

3.1.3. Climate

The IJsselmeer experiences temperate climatic conditions. This is defined by the convergence of two air masses thus the humid maritime air mass from the west and the dry continental air mass from the east (UNEP, 2009). The coming together of these air mass results in mild winters and cooler summers.

3.1.4. Socioeconomic Characteristics

The location of IJsselmeer and its' climatic condition makes it a very important fresh inland water body. It serves as a source of food and income and also a main source of recreation. The reclamation of the 'Zuider Zee' in 1937 has seen the lake been used in the production of different spices of fish. For instance pike, peach and eels. It has also created a source of employment for residents around the lake (Dekker, 1993; Lorenzoni et al., 2015; The Columbia Encyclopedia, 6th ed., 2015).

IJsselmeer also serves as a perfect holiday ground for all ages of people, the region is characterised by pleasant beaches, busy locks and comes with an array of water sporting facilities (Huitema, 2002; TheIJsselmeer.com, 2016). In recent times, the lake is been exploited as a source of generating electricity. The introduction of REDStack's blue energy is but one of the many projects within the catchment area of the lake where research is being done to exploit the potential of generating electricity (Holland.com, 2014; Huitema, 2002).

3.2. DESCRIPTION OF DATA

3.2.1. Field measurement

Field measurement conducted for this research were of three different types. The actual field visit and ancillary data collection, data collection from independent also referred to as secondary data and the actual field measurements with the WISP-3 spectrometer. The subsequent section gives a detail description of the various measurement and data collected.

3.2.1.1. Field Campaign

Field measurement was undertaken by Chawira, (2012) for an ITC thesis. The data primarily consist of radiometric measurement of the IJsselmeer using the WISP-3 spectrometer (Water insight, 2015). Three fields campaigns were conducted for the month of September 2011, on the following days: 23rd, 25th and on the 28th. Data of the 23rd and 25th generally were obtained on cloudy days, while data obtained on the 28th were on a cloud free day.

Table 3-1. Field days and the number of field measurement conducted on those days.

Date	Number of Samples

23rd September 2011	8
25th September 2011	11
28th September 2011	22
Total	**41**

Table 3-1 above indicates the number of samples that were collected for each of the days of field campaign, in total 41 sampled sites were covered. The spatial coordinates for some locations were recorded with the Garmin etrex global positioning system (GPS).

Ancillary data were also collected on the 28th of September 2011. These data include Secchi disk measurement, wind speed, water temperature and sea level pressure. Table 3-2 below gives further details of the measurements taken on this day.

Table 3-2. Ancillary data from 28th September 2011

Date	Parameter	Measurement	Units (Symbol)
28th September 2011	Secchi disk depth	1.5	Meters (m)
	Wind speed	4	Meters per second (m/s)
	Water temperature	15.8	Degree Celsius (°C)
	Sea level pressure	1033	Hector pascal (hPa)

3.2.1.2. PC Fluorescence

An independent dataset was acquired of the IJsselmeer from the Rijwaterstaat an arm of the Royal Dutch Ministry of Transportation and Water Management. This data consist of two geographic points within the IJsselmeer known as Pole 46 and 47 with geographic coordinate at longitude 5.492902, Latitude 52.70991 and Longitude 5.223987 and Latitude 52.91201 respectively. The data collected at the poles includes; turbidity, water temperature, oxygen, Chl-a and PC fluorescence. Varied instruments were used in measuring the various water quality parameters at the poles. Below in Table 3-3 is the breakdown of the type of instruments used in performing the measurement with their units of measurement.

Table 3-3. Summary of water quality variables and their corresponding measuring instruments and Units for the poles within the lake.

Water quality variable	Instrument	Unit
PC pigment	YSI 6131 phycocyanin Blue-green sensor	RFU
Turbidity	YSI 6136 turbidity sensor	NTU
Oxygen	ROX optical sensor	Mg/L
Chlorophyll	YSI 6025 sensor	Mg/L
Temperature	130 EcoSense Temperature Sensor	°C

RFU (Relative Fluorescence Unit), is a unit of measure used in analysis involving fluorescence detection (Gertsch et al., 2002). RFU was used as a standard of measure in this work. NTU, on the other hand, refers to Nephelometric Turbidity Unit. It measures scattered light at 90 degrees to the incident beam and is detected by a single detector. The range of NTU for broadband peaks at spectral outputs of 400 nm to 680 nm (USGS, 2013).The data from these poles were measured every 10 minutes for the various water quality parameters.

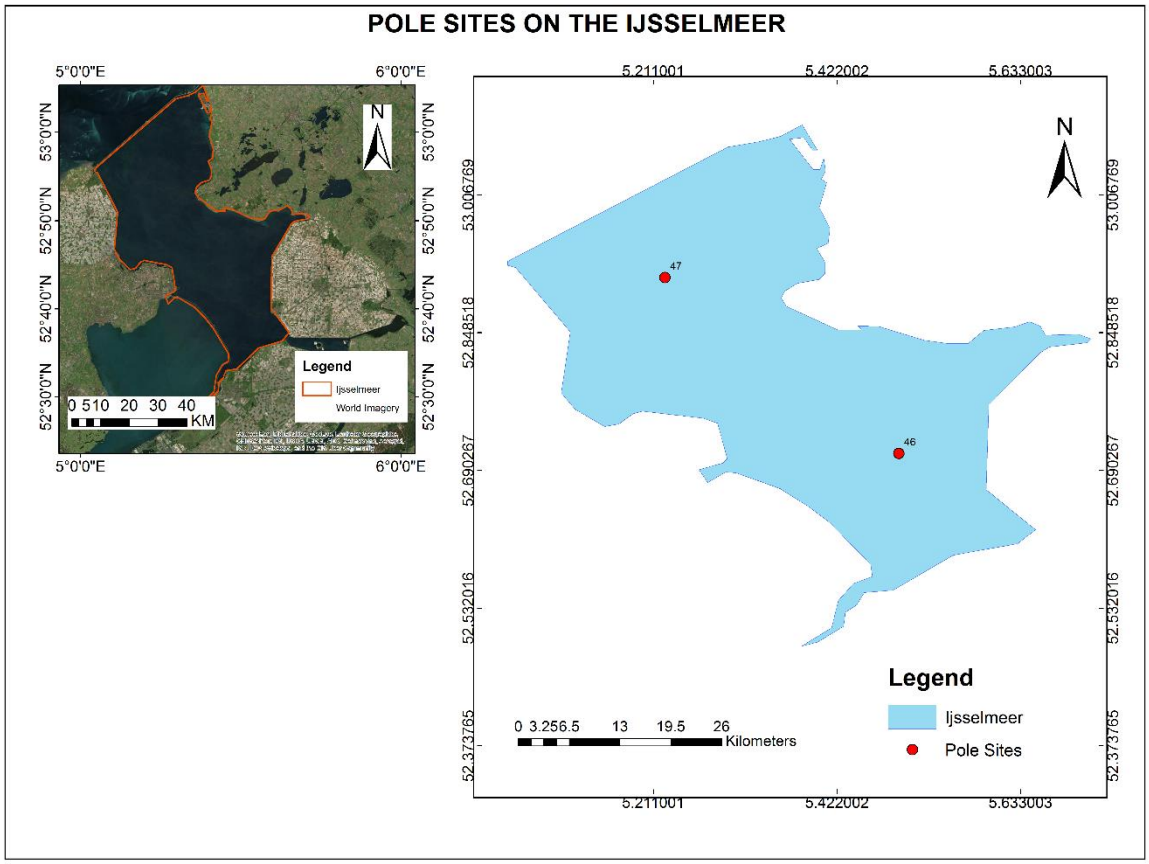

Figure 3-2. Map of the study area showing the locations of poles on the IJsselmeer from which measurements were taken.

3.2.1.3. WISP-3 Data

WISP-3 data were subdivided into three for each day that field measurements were carried out thus 23rd, 25th and 28th of September, 2011. Raw data from the WISP-3 spectrometer measures sky radiances, water radiance and irradiance. WISP-3 has the following physical and spectral properties.

Table 3-4 Properties of the WISP-3 instrument

Property	Measurement range
Measuring time	0.2 – 2 minutes
Field of view	3° (Default)
SNR	250:1
Operational range	-5°C - 45°C (Default)
Calibrated spectral range	350 – 800 nm
Spectral bandwidth	~4.9 nm

Data for the 23rd of September, 2011, were taken between Enkhuizen to Stavoren Section of the lake. In total 8 samples were taken on this day at different time intervals. The data consisted of downwelling sky radiance (L_d), upwelling water surface radiance (L_u) and downwelling sun/sky irradiance (E_d). Below are the graphical representations of the data as measured by the WISP-3 spectrometer.

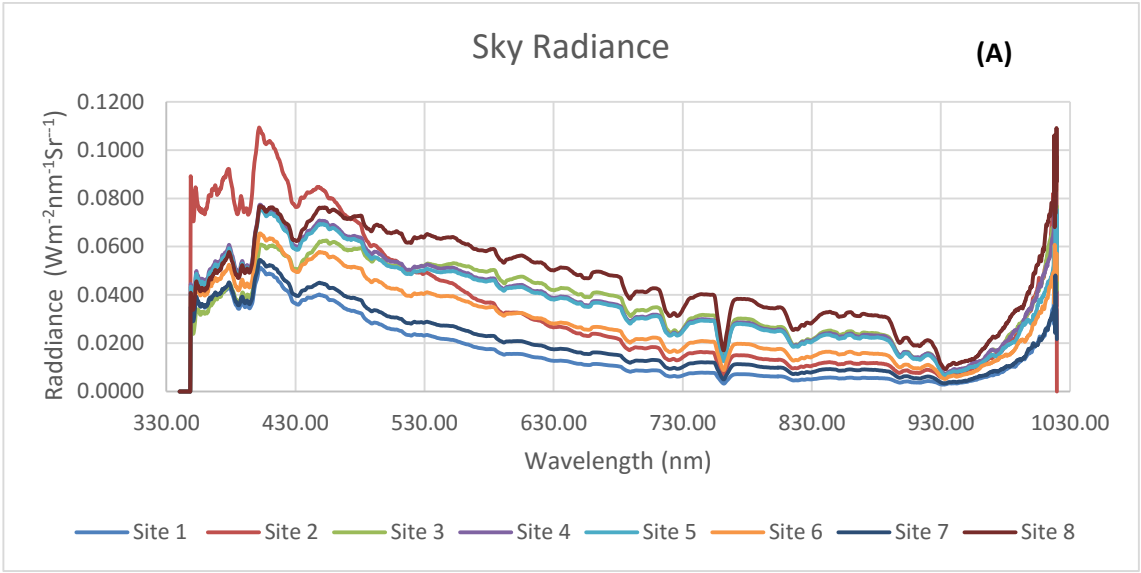
Sky Radiance
(A)
Raddiance (Wm-2nm-1Sr-1)
0.1200
0.1000
0.0800
0.0600
0.0400
0.0200
0.0000
330.00
430.00
530.00
630.00
730.00
830.00
930.00
1030.00
Wavelength (nm)
Site 1
Site 2
Site 3
Site 4
Site 5
Site 6
Site 7
Site 8

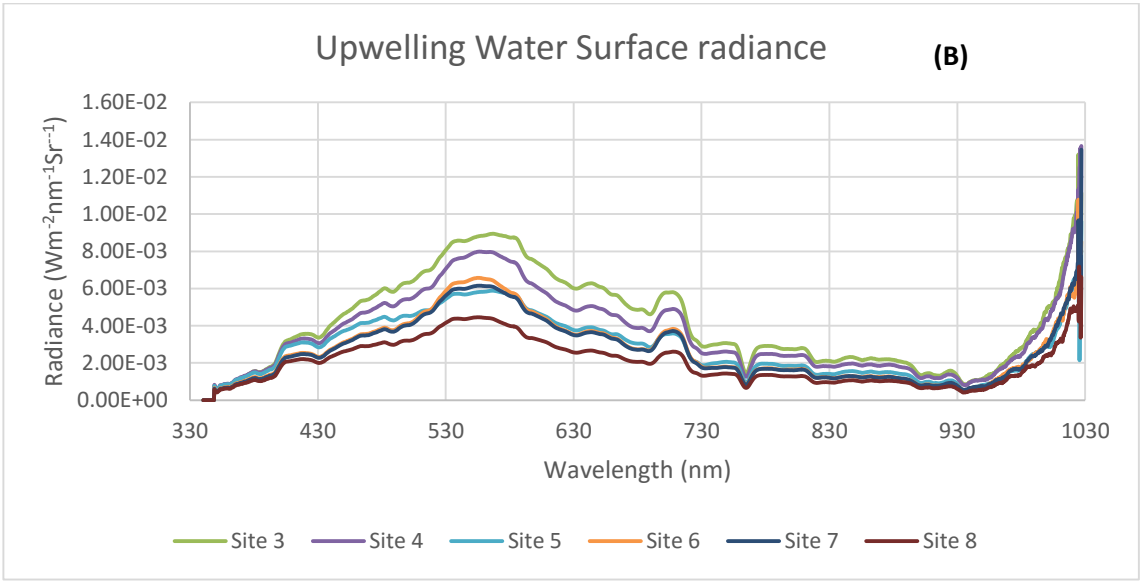
Upwelling Water Surface radiance
(B)
Radiance (Wm-2nm-1Sr-1)
1.60E-02
1.40E-02
1.20E-02
1.00E-02
8.00E-03
6.00E-03
4.00E-03
2.00E-03
0.00E+00
330
430
530
630
730
830
930
1030
Wavelength (nm)
Site 3
Site 4
Site 5
Site 6
Site 7
Site 8

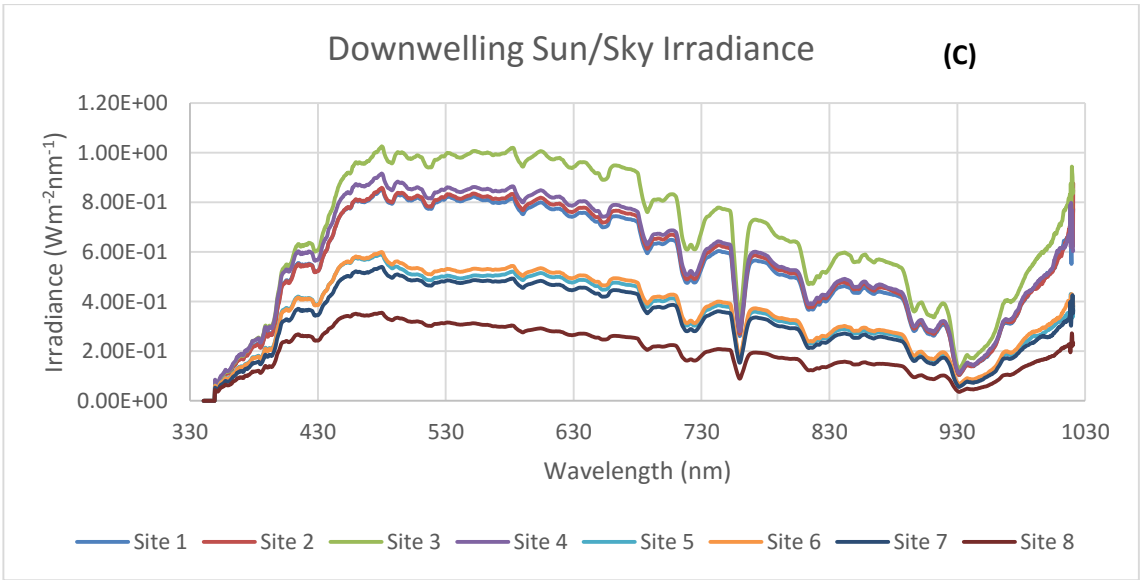
Downwelling Sun/Sky Irradiance
(C)
Irradiance (Wm-2nm-1)
1.20E+00
1.00E+00
8.00E-01
6.00E-01
4.00E-01
2.00E-01
0.00E+00
330
430
530
630
730
830
930
1030
Wavelength (nm)
Site 1
Site 2
Site 3
Site 4
Site 5
Site 6
Site 7
Site 8

Figure 3-3. Raw WISP measurement for 23rd September 2011. Figure 3-3 (A) is Sky radiance Figure 3-3 (B) is Upwelling water Surface radiance. This figure eliminates sites 1 ad 2 as the data from these sites were outliers and Figure 3-3 (C) is downwelling sun/sky irradiance

Data for 25th of September, 2011 is presented below as measured by the WISP-3 spectrometer. The measurements for this day were close the Enkhuizen to Stavoren measurements.

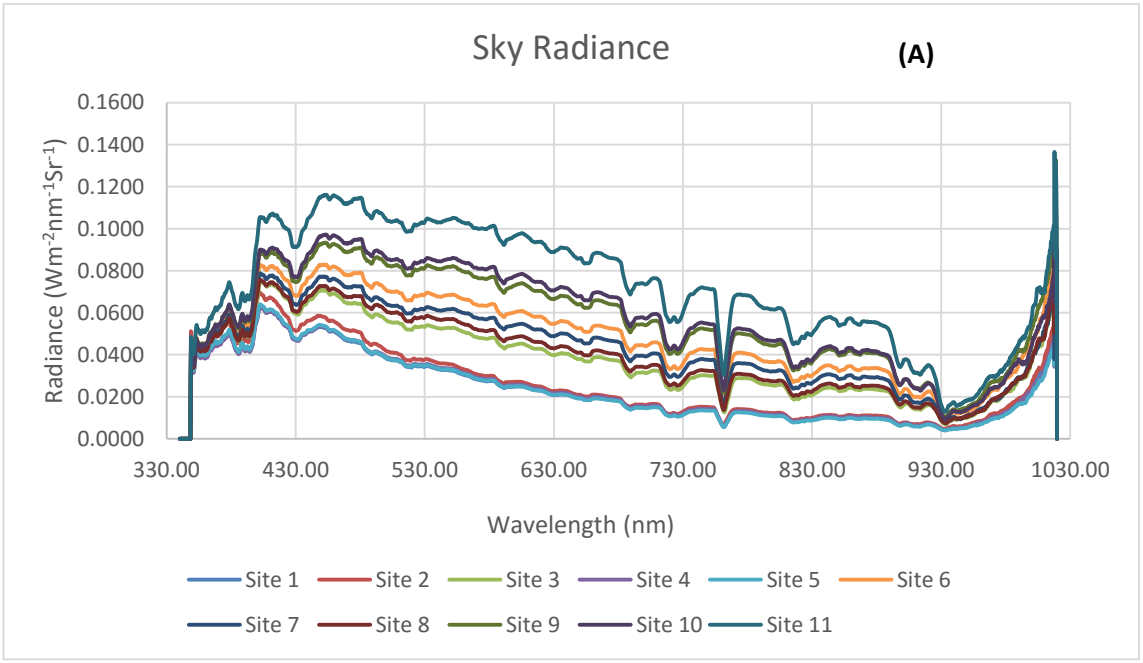

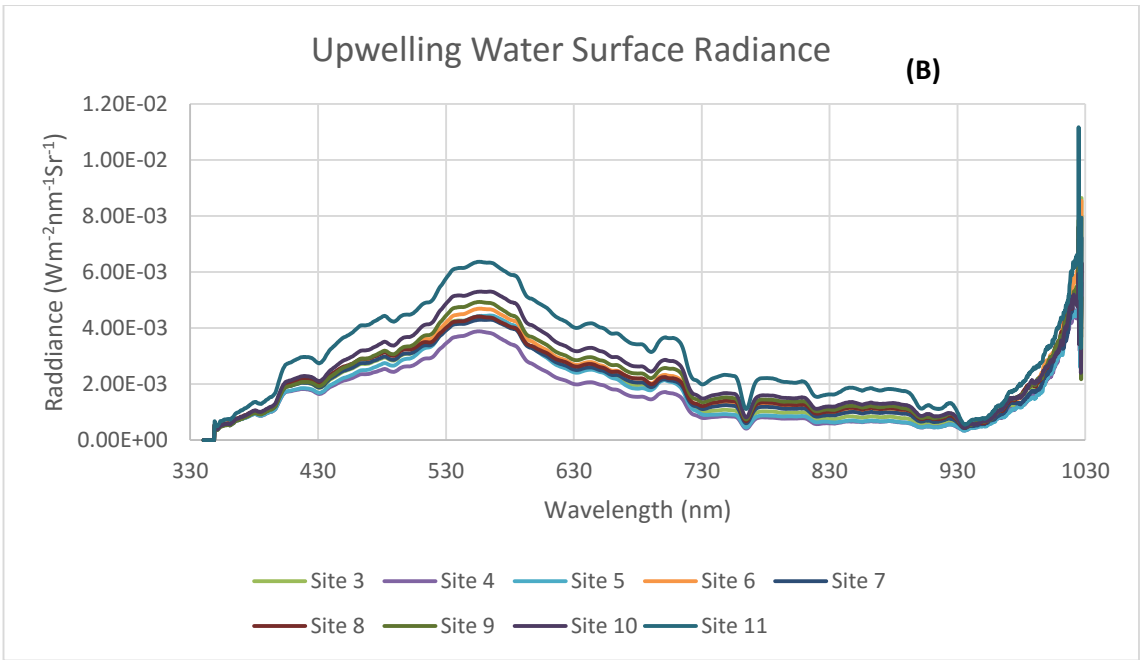

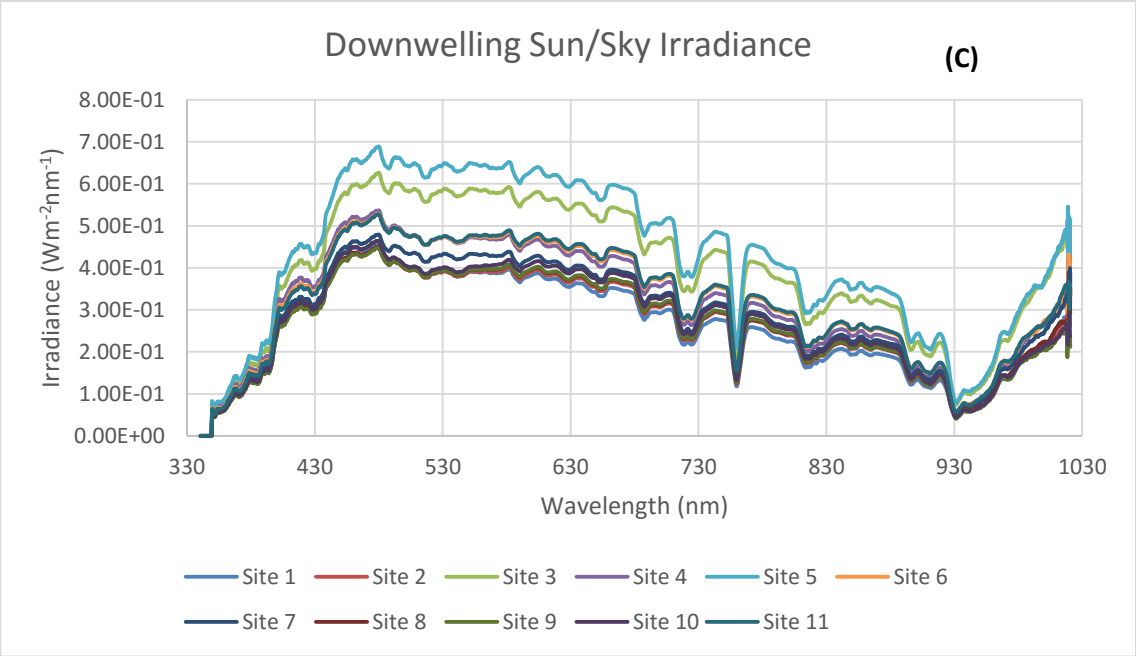

Figure 3-4. Raw WISP measurement for 25th September 2011. Figure3-4 (A) is Sky radiance (B) is upwelling water surface radiance from which sites 1 and 2 were eliminated and (C) is downwelling sun/sky irradiance

The other field campaigned covered the northwestern part of the lake between Enkhuizen and Den Oever. The campaign produced 22 samples. A graphical representation of this data is detailed below.

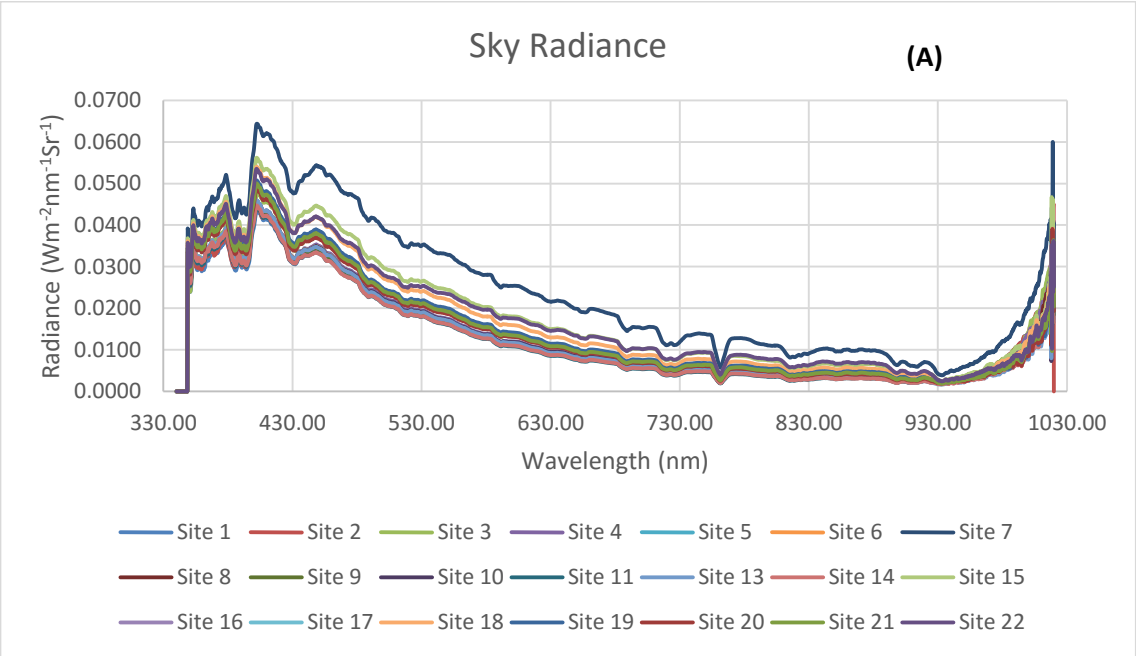

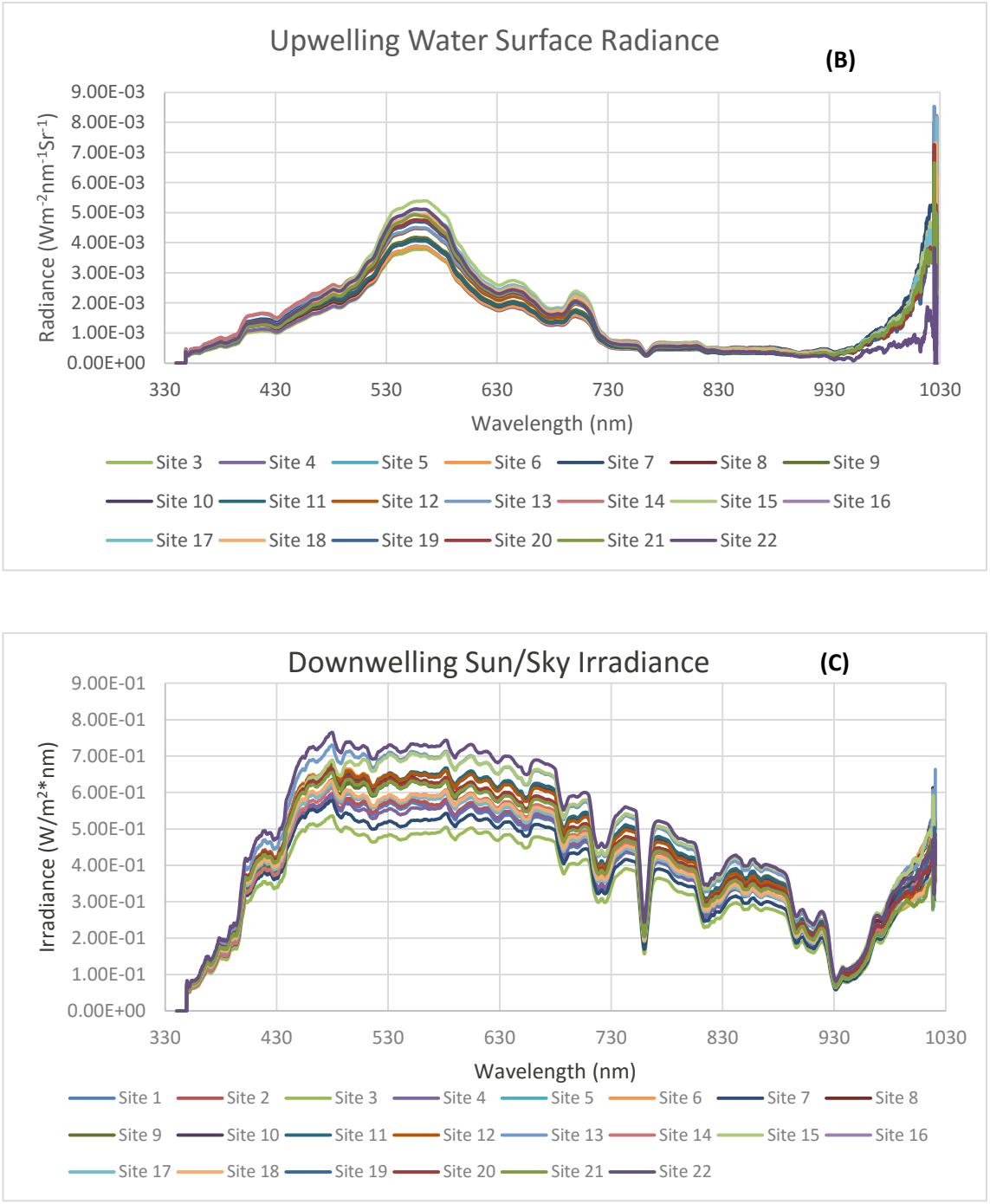

Figure 3-5. Raw WISP measurement for 28th September 2011. Figure 3-5 (A) is Sky radiance (B) is upwelling water surface radiance eliminating sites 1 and 2 and (C) is downwelling sun/sky irradiance

Some outlier effects were observed in figures 3-3 (B), 3-4 (B) and 3-5 (B). These outliers could be as a result of floating chips on the water, the difference in the viewing angle of the WISP-3 spectrometer among others (Sun et al., 2015). As a result of this, these outliers were dropped from the datasets and only valid spectra were used for the research. Figure 3-6 below is a description of the study site from which samples were collected.

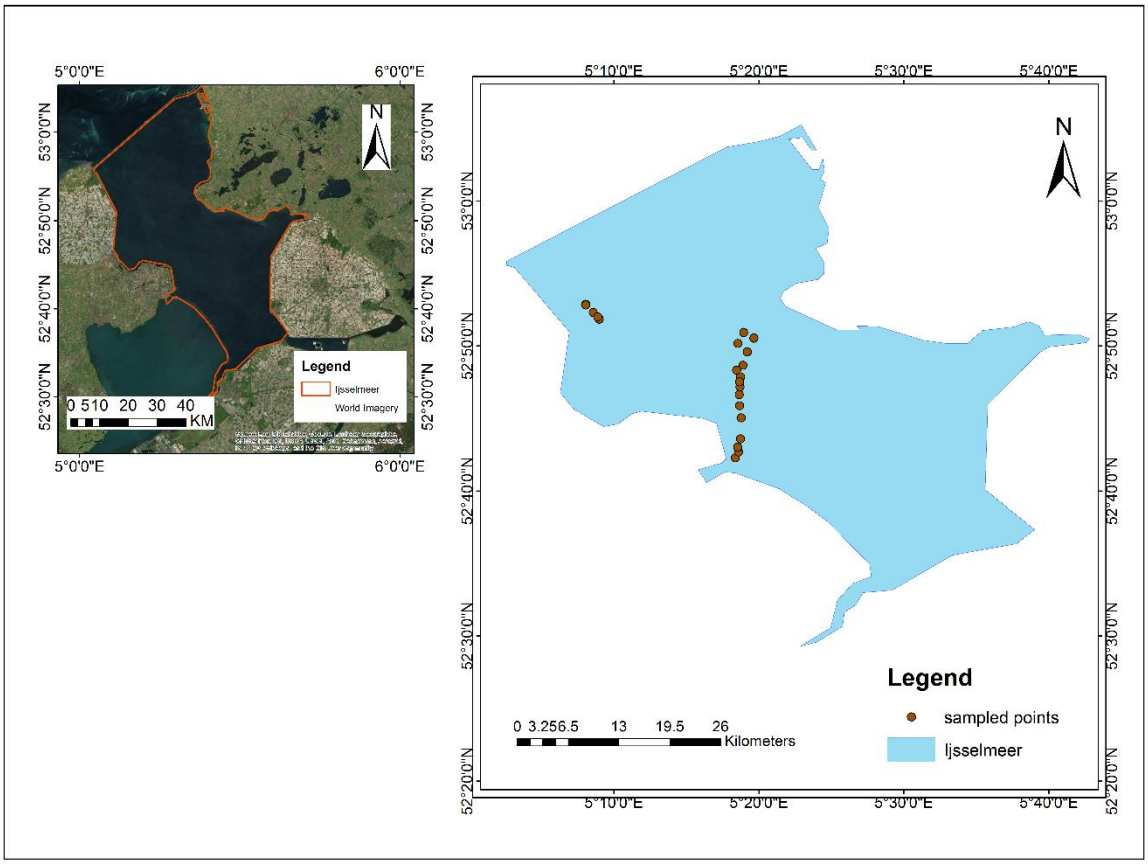

Figure 3-6. Map of the study area with sampled sites from which field sampling was conducted

3.2.2. Satellites Data

Satellite data were obtained from Landsat 8 OLI and Sentinel-2 MSI for this study. Data from Landsat 8 OLI were obtained from the United State Geological Survey (USGS) online portal of the study area that is http://earthexplorer.usgs.gov/ whiles images of Sentinel 2 were obtained from the European Space Agency (ESA) data hub that is https://scihub.esa.int/dhus/.

3.2.2.1. Landsat 8 OLI data

Landsat 8 OLI has 9 spectral bands each with specific tasks and type. The satellite has a different spectral width and spatial resolutions. The sensor is generally characterized by a 30-meter spatial resolution with one 15 meter resolution at band 8 the Panchromatic band. Below in table 3-5 is a describing the spatial and spectral characteristics of Landsat 8 OLI sensor. Followed by the spectral response function of the sensor in figure 3-7.

Table 3-5. Landsat 8 OLI spectral characteristics

Band Number	Type	Centre λ (nm)	Spectral width Δλ (nm)	Spatial Resolution (m)
Band 1	Coastal/Aerosol	442.96	15.98	30
Band 2	Blue	482.04	60.04	30
Band 3	Green	561.41	57.33	30
Band 4	Red	654.59	37.47	30
Band 5	NIR	864.67	28.25	30

Band 6	SWIR-1	1608.86	84.72	30
Band 7	SWIR-2	2200.73	186.66	30
Band 8	Pan	589.50	172.40	15
Band 9	Cirrus	1373.43	20.39	30

Below is the spectral responses function of Landsat 8 OLI as published by the USGS.

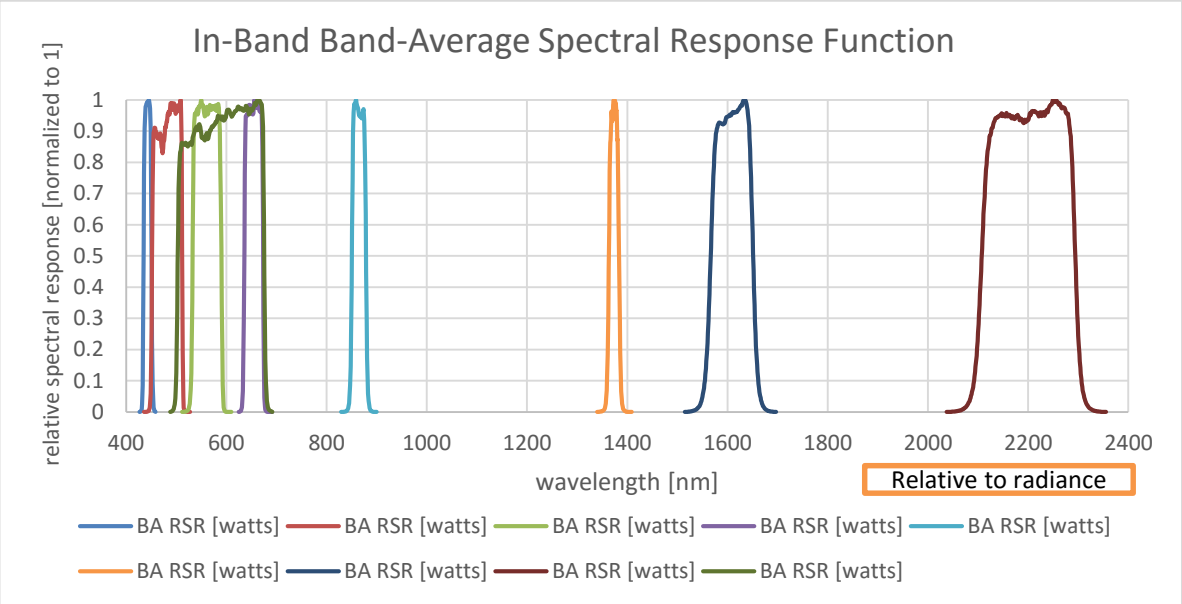

Figure 3-7. Spectral response function of Landsat 8 OLI

3.2.2.2. Sentinel-2 MSI

Sentinel-2 MSI has 13 spectral channels. The sensor is characterized by a large spatial resolution ranging from 10 to 60 meters. It has 4 channels at 10-meter resolution, 6 channels at 20 meters and 3 channels at 60 meters resolution. One of the Channels thus band 8 is divided into two (2) band 8 in the 10-meter resolution range and band 8a in the 20-meter resolution range. The division of this band is to cater for individual parameters, like leaf area index, water vapour absorption reference, retrieval of aerosol load and type etc. It has a revisit time of 15 days and as a term of constellation allows for 5 days revisit time (Berthelot & Santer, 2009). Below in Table 3-6 is a depiction of the spectral and spatial characteristics of Sentinel-2 MSI satellite followed by the spectral responses function of the sensor in Figure 3-8.

Table 3-6. Sentinel-2 MSI spectral characteristics

Band number	Central wavelength (nm)	Bandwidth (nm)	Spatial resolution (m)	L_{ref} (W m^{-2} sr^{-1} μm^{-1})	SNR L_{ref}
1	443	20	60	129	129
2	490	65	10	128	154
3	560	35	10	128	168
4	665	30	10	108	142
5	705	15	20	74.5	117
6	740	15	20	68	89
7	783	20	20	67	105
8	842	115	10	103	174

8a	865	20	20	52.5	72
9	945	20	60	9	114
10	1380	30	60	6	50
11	1610	90	20	4	100
12	2190	180	20	1.5	100

(Drusch et al., 2012)

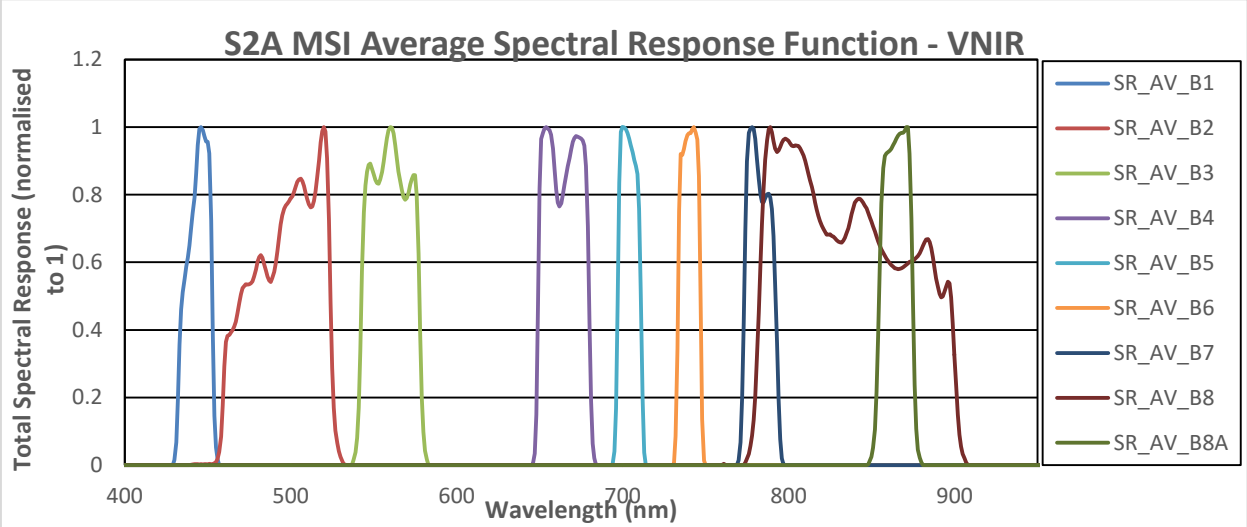

Figure 3-8. Spectral responses function of Sentinel-2 MSI

Source:https://sentinel.esa.int/web/sentinel/sentinel-2-msi-wiki/-/wiki/Sentinel%20Two/Performance

A description of the Sentinel-2 MSI sensor by bands and the purpose of the bands is given in table 3-7 below.

Table 3-7. Description of Sentinel-2 MSI spectral bands

Band	Centre λ (nm)	Spectral Width Δλ (nm)	Spatial Resolution (m)	Purpose
1	443	20	60	Atmospheric Correction
2	490	65	10	Sensitive to Vegetation Aerosol Scattering
3	560	35	10	Green peak, sensitive to total chlorophyll in vegetation
4	665	30	10	Max Chlorophyll absorption
5	705	15	20	Position of red edge consolidation of atmospheric correction, / fluorescence retrieval of aerosol
6	740	15	20	Position of red edge atmospheric correction, retrieval of aerosol
7	775	20	20	LAI ,edge of NIR plateau
8	842	115	10	LAI
8b	865	20	20	NIR plateau, sensitive to total chlorophyll biomass, LAI and protein; water vapour absorption reference; retrieval of aerosol load and type
9	940	20	60	Water Vapour absorption atmospheric correction
10	1375	20	60	Detection of thin cirrus for atmospheric correction
11	1610	90	20	Sensitive to lignin, starch and forest above ground biomass snow/ice/cloud separation
12	2190	180	20	Assessment of Mediterranean vegetation conditions. Distribution of clay soils for the monitoring of soil erosion. Distribution of live biomass, dead biomass and soil, e.g. for bum scars mapping.

(Berthelot & Santer, 2009)

4. METHODOLOGY

4.1. Field data management

WISP-3 data collected in the field were in different wavelength ranges and first had to standardize. This process was done by interpolating the WISP data to match with that of Landsat 8 OLI. The data was interpolated to 1 nm interval to match the multispectral instruments spectral response function (SRF).

4.2. Remote Sensing Reflectance (R_{rs})

WISP data for the sampled sites were prepared together with ancillary data to calculate remote sensing reflectance (R_{rs}). The measurement for each sampled pointed contained three properties. Sky radiance, upwelling water surface radiance and downwelling sun/sky irradiance. Based on these properties and field measurement protocols (Gons et al., 2005; Mueller et al., 2003) WISP-3 above surface irradiance reflectance was computed.

$$R(0+) = \left(\frac{L_{uw}(\lambda) - \rho * L_{sky}(\lambda)}{E_d(\lambda)}\right) * n_w^2 * Q \qquad \text{Equation 1}$$

Where; $L_{uw}(\lambda)$ is upwelling water surface radiance ($Wm^{-2}nm^{-1}sr^{-1}$), $L_{sky}(\lambda)$ is sky radiance ($Wm^{-2}nm^{-1}sr^{-1}$), Ed (λ) is downwelling sun/sky irradiance ($Wm^{-2}nm^{-1}$), ρ is direct surface reflectance with a value of 0.22, n_w is the index of refraction between water and air with a value of 1.33 and Q is the conversion factor for upwelling surface radiance to upwelling subsurface irradiance. For isotropic light fields, the conversion factor is taken to be pi (π).

To obtain the upwelling subsurface irradiance, the following equation was applied

$$L_u(0+) = n_w^2 * Q * \left[L_{uw}(0+) - \rho * L_{sky}(0+)\right] * (1 - \rho - w) \qquad \text{Equation 2}$$

Downwelling sun/sky radiance was also converted to subsurface irradiance as follows

$$E_d(0, \lambda) = E_d(0+) + 0.5 * E_u(0-) \qquad \text{Equation 3}$$

The equation of Mobley, (1999) was applied in calculating $R_{rs}(\lambda)$ on the surface of the lake. R_{rs} (λ) was calculated as the ratio of upwelling water leaving radiance (L_{uw} (λ)) and downwelling irradiance (E_d (λ)) as shown in the equation below.

$$R_{rs} = {}^{L_u}/_{E_d} \qquad \text{Equation 4}$$

Below is a summary of the methodology

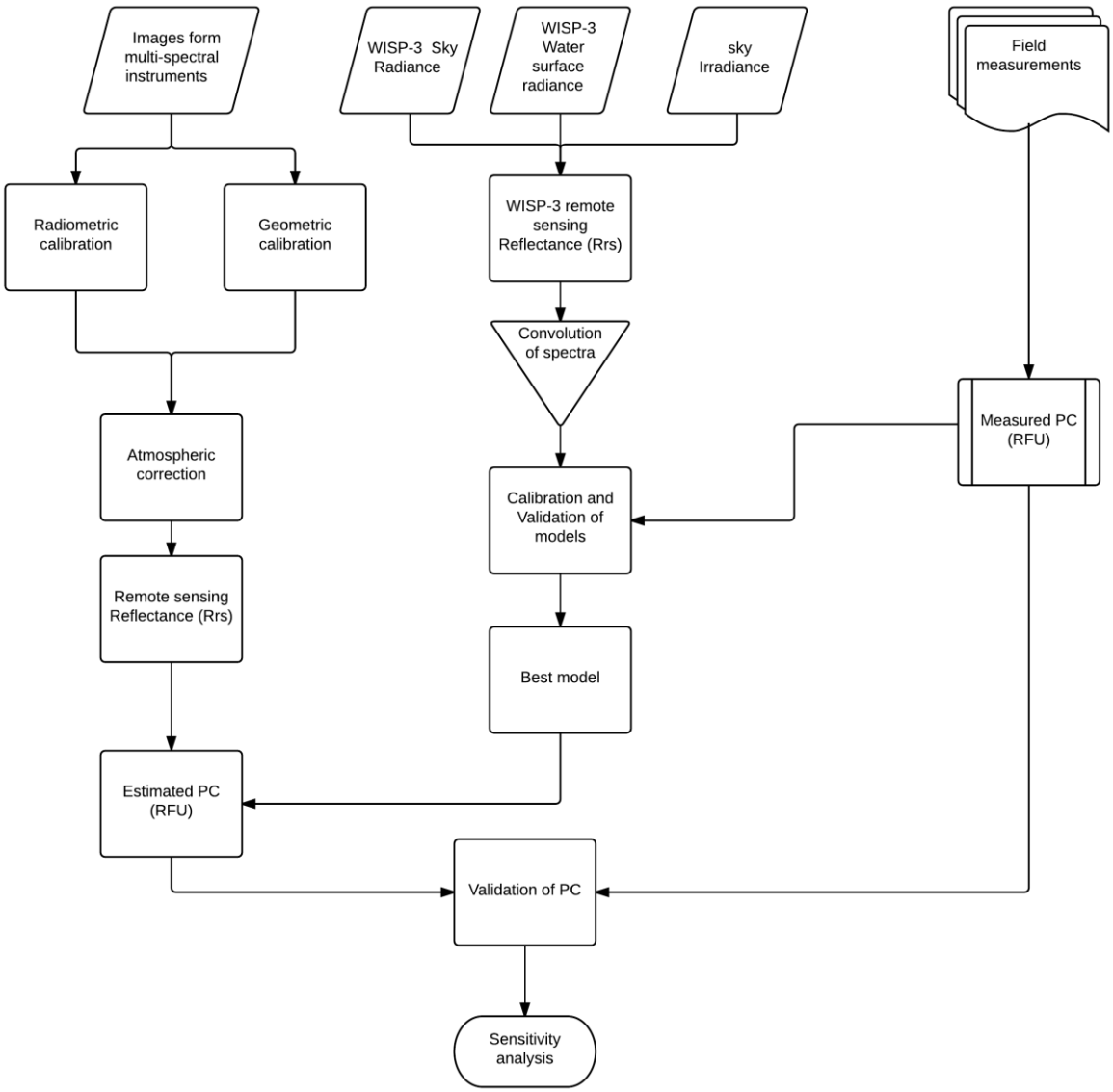

Figure 4-1. Flowchart for the study

4.3. Convolve Rrs(λ) data to Landsat 8 OLI spectra

The WISP-3 remote sensing data were convolved into multispectral instrument spectra. This process was to match up the measurement taken by the spectrometer (WISP-3) to Landsat 8 OLI. This was achieved by applying the following equation

$$R_{rs}(Band_i) = \frac{\int_{lower\,\lambda}^{upper\,\lambda} SRF(\lambda) * R_{rs(in-situ)}(\lambda) d\lambda}{\int_{lower\,\lambda}^{upper\,\lambda} SRF(\lambda) d\lambda} \quad \text{Equation 5}$$

Where $R_{rs}(Band_i)$ is the remote sensing reflectance of the i^{th} band of sensor and $d\lambda$ is the change in wavelength, $R_{rs(in-situ)}$ is the in-situ measured remote sensing reflectance and SRF is the spectral response function. So the Upper and lower limits of the spectra are involved in the integration process.

In convolving the field measured $Rrs(\lambda)$ to Landsat 8 OLI spectra the following bands were considered as shown in table 4-1 below.

Table 4-1. Landsat 8 OLI convolution bands and band range

Satellite	Bands	Type	Band Range (nm)	Central Band (m)
Landsat 8 OLI	1	Coastal Aerosol	427 - 459	443
	2	Blue	436 – 528	489
	3	Green	512 – 610	561
	4	Red	625 – 691	658
	5	NIR	829 – 900	864.7

Source; (USGS, 2015)

After applying the above-mentioned equation, the WISP-3 data would now fall within the range of the Landsat 8 OLI spectra. The newly generated data was then applied to the selected models as measurement obtained in the fields of view of Landsat 8 OLI. The application of the model takes the central bands of the band range.

4.4. Convolve Rrs(λ) data to Sentinel-2 MSI Spectra

The WISP-3 data was processed and convolved into Sentinel-2 MSI spectra. This involves the use of equation 2 and the application of the process briefly explained in section 4.3 above. The following bands were used in performing the convolution.

Table 4-2 Sentinel - 2 MSI convolution bands

Satellite	Band	Type	Central Band (nm)	Resolution (m)
Sentinel-2 MSI	1	Ultra-blue	443	60
	2	Blue	490	10
	3	Green	560	10
	4	Red	665	10
	5	VNIR	705	20

The process of convolving data collected in the field to Multispectral instruments spectra also known as data matchup is to bring the data from the field to the field of view of the multispectral instrument. Data matched-up into the multispectral instrument spectra, are then used to calculate PC in the eye of the multispectral instrument.

4.5. Calibration of selected models for the IJsselmeer

A multivariate regression model was applied on field data to generate model coefficients for the calibration of the models. In-situ data with their corresponding PC sites were subdivided into calibration and validation sets. This was done by applying GeoCalVal model by Salama et al. (2012) on the datasets 60% of the data was used for calibration whiles 40% was used for Validation.

The first model calibrated was by Sun et al. (2015). The model equation is briefly described below.

$$PC = K_0 + K_1 R_{rs}(b1) + K_2 R_{rs}(b2) + K_3 R_{rs}(b3) + K_4 R_{rs}(b4) + K_5 \left(R_{rs}\left(\frac{b4}{b3}\right)\right) + K_6 \left(R_{rs}\left(\frac{b4}{b2}\right)\right) + K_7 \left(R_{rs}\left(\frac{b4}{b1}\right)\right) + K_8 \left(R_{rs}\left(\frac{b3}{b2}\right)\right) + K_9 \left(R_{rs}\left(\frac{b3}{b1}\right)\right) + K_{10} \left(R_{rs}\left(\frac{b2}{b1}\right)\right)$$

Equation 6

Where: b1, b2, b3 and b4 denotes bands 1, 2, 3 and 4 respectively and $K_0 - K_{10}$ were used as model coefficients from the multivariate regression.
The second model developed by Vincent et al. (2004) was also calibrated. The model equation is shown below.

$$PC = K_0 - K_1\left(R\frac{B3}{B1}\right) + K_2\left(R\frac{B4}{B1}\right) - K_3\left(R\frac{B4}{B3}\right) - K_4\left(R\frac{B5}{B3}\right) + K_5\left(R\frac{B7}{B3}\right) - K_6\left(R\frac{B7}{B4}\right)$$

Equation 7

Where $K_0 - K_6$ represents the model coefficients, B1, B3, B4, B5 and B7 are bands 1, 3, 4, 5 and 7 respectively. It was observed that the model does not include band 2. This model was originally designed for Landsat thematic mapper (Landsat (TM)). This model was also observed to have a considerable amount of PC absorption between band 2 and 3, so to compensate for the loss of information within that range, a band ratio of bands 3 and 1 was used instead. The reason being that the spectral curves of these bands are approximately equal (Vincent et al., 2004). Therefore band 2 was not used in the estimation of PC.
Vincent et al. (2004) model included band 7 of the sensor. This band is a Shortwave infrared band (SWIR (2080 nm – 2350 nm) which is a band that accounts for the extinction coefficients as wavelength increases. During the model application, the model had to be recalibrated to suit the sensors. This was done to accommodate for the WISP-3 instrument range. The model calibration therefore eliminated the SWIR band from the original model and a modified version of the model was used instead as shown below.

$$PC = K_0 - K_1\left(R\frac{B3}{B1}\right) + K_2\left(R\frac{B4}{B1}\right) - K_3\left(R\frac{B4}{B3}\right) - K_4\left(R\frac{B5}{B3}\right)$$

Equation 8

4.6. Comparing and Validation of models

Type II linear regression was applied to the models for validation. Mean absolute percentage error (MAPE), root mean square error (RMSE) and coefficients of determination (R^2) were used to check the model accuracy. The best performing model was therefore selected and adopted for the IJsselmeer.

4.7. Application of selected model on the multispectral instruments.

In applying the model, atmospheric correction was performed using the Fast Line-of-Sight Atmospheric Analysis of the spectral (FLAASH) model. This model accounted for atmospheric influences sure as molecules, particulate scattering, surface caps etc. (Felde et al., 2003; Gordon & Franz, 2008). The subsequent section described the application process for the atmospheric correction model.

4.7.1. Atmospheric correction using FLAASH

The Fast Line-of-Sight Atmospheric Analysis of the spectral Hypercubes (FLAASH) model in ENVI was used for correcting atmospheric effects as mentioned in the preceding section. The application of the atmospheric correction is to address issues of illumination, atmospheric influences and terrain correction. FLAASH applies the following equations in performing atmospheric correction.

$$L = \left(\frac{A\rho}{1-\rho_e S}\right) + \left(\frac{B\rho_e}{1-\rho_e S}\right) + L_a$$

Equation 9

Where:
ϱ is the pixel surface reflectance
ϱ_e is an average surface reflectance of the pixel and a surrounding region
S is spherical albedo of the atmosphere

L_a is the radiance backscattered by the atmosphere
A and B are coefficients that depend on the atmospheric and geometric conditions but not on the surface as noted by I T T Visual Information Solutions, (2009). The above-mentioned equation is used in retrieving the pixel surface reflectance. Knowing the pixel surface reflectance, spatially averaged reflectance (ρ_e) is estimated using an approximate equation which is shown below.

$$L \cong \left(\frac{(A+B)\rho_e}{1-\rho_e S}\right) + L_a \qquad \text{Equation 10}$$

For Sentinel-2 MSI, it was noticed that the band selection for atmospheric correction is different from the bands that were required for calculating PC. Table 4-3 below presents the suitable bands for atmospheric correction in Sentinel-2 MSI.

Table 4-3 Sentinel-2 MSI spectra band specification

Spectral bands (Centre wavelength in nm/SSD in m)	Mission objective	Measurement or calibration
B1 (443/20/60), B2 (490/65/10) and B12 (2190/180/20)	Aerosols correction	Calibration bands
B8 (842/115/10), B8a (865/20/20), B9 (940/20/60)	Water vapour correction	
B10 (1375/20/60)	Circus detection	
B2 (490/65/10), B3 (560/35/10), B4 (665/30/10), B5 (705/15/20), B6 (740/15/20), B7 (775/20/20), B8 (842/115/10), B8a (865/20/20), B11 (1610/90/20), B12(2190/180/20)	Land cover classification, Leaf chlorophyll content, leaf water content, LAI, fAPAR, snow/ice/cloud, mineral detection.	Land measurement bands

Source: (European space agency, 2012)

4.7.2. Application of selected model on atmospherically corrected images

The adopted model was applied on the multispectral instruments and PC in relative fluorescence units (RFU) were retrieved. This was achieved using the band maths tool in ENVI. An accuracy assessment was then performed. This assessment was aimed at validating the measured PC from in-situ observed PC in RFU. For the application of the model, band 1 of Landsat 8 OLI which is a coastal aerosol band was eliminated leaving bands 2, 3, 4 and 5 as bands 1, 2, 3 and 4 respectively for the model.

4.8. Sensitivity Analysis

Statistical comparison was carried out to ascertain the accuracy of the results obtained. Some of the statistical variables that were calculated include: the mean absolute percentage error (MAPE), the root mean square error (RMSE), the coefficient of determination (R^2) and in some instances the coefficient of correlation (R).

$$R^2 = 1 - \frac{SS_{res}}{SS_{Tot}} \qquad \text{Equation 11}$$

So SS_{res} represented the sum of the square of residuals and SS_{Tot} is the total of the sum square.
The RMSE is a measure of the average squared distance of data to a fitted line. The calculation of RMSE is shown below:

$$\text{RMSE} = \sqrt{\left(\frac{1}{n-1}\sum_{i=1}^{n}\left(PC_{Image,i} - PC_{in-situ,i}\right)^2\right)} \qquad \text{Equation 12}$$

Where; $PC_{image,I}$ represented the PC derived from the image and $PC_{in\text{-}situ,I}$ represented PC derived from in-situ measurement.

MAPE is an average of the absolute value of residual in percentage. It is less sensitive to large errors as shown in the formula below:

$$\mathrm{MAPE} = \frac{100}{\mathrm{n}} \sum_{\mathrm{i}=1}^{\mathrm{n}} \left| (\mathrm{PC}_{in-situ,i} - \mathrm{PC}_{\mathrm{derived,i}}) / PC_{in-situ,i} \right| \qquad \text{Equation 13}$$

$PC_{in\text{-}situ,i}$ represented measured PC from the field whiles $PC_{derived,i}$ was PC as derived from the satellite images. MAPE was used to measure the closeness of the derived PC concentration to the in-situ measured PC in percentage.

5. RESULTS AND DISCUSSION

5.1. PC Fluorescence

PC fluorescence measurements were recorded from pole 46 located in the south-eastern portion of the lake and pole 47 in the North West. Figure 5-1 below shows PC fluorescence for the three field campaign days. It was observed that, there was a wide variation in the measurement on the 23rd of September 2011 than any of the other days. This could be attributed to the weather conditions on this particular day as the day was generally cloudy as described in Section 3.2.1.

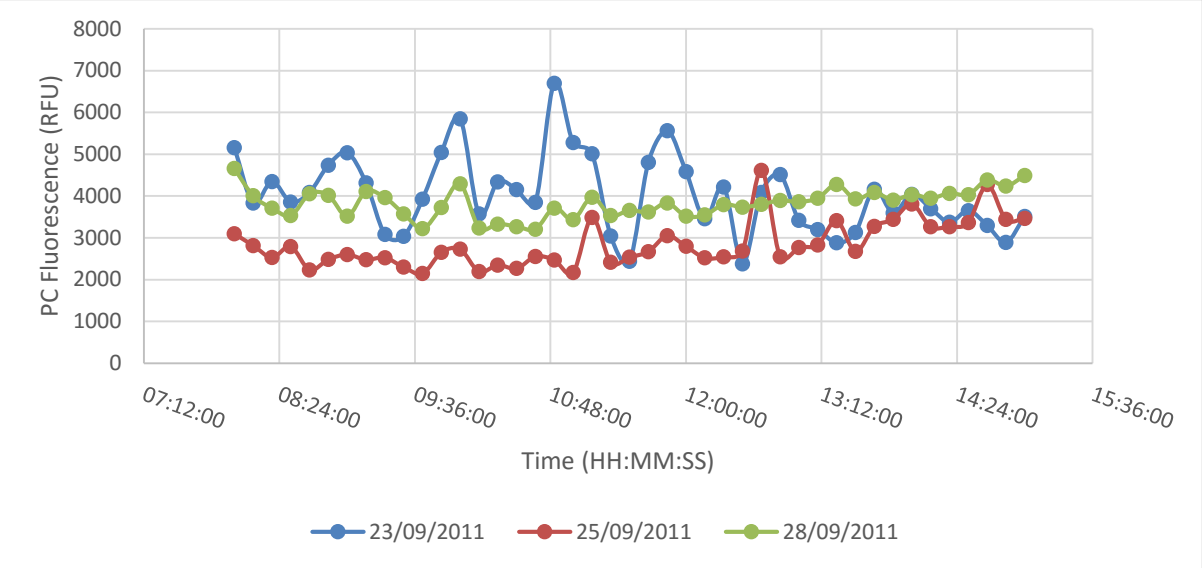

Figure 5-1. Combined plot of the three sampling days. This figure represented the variation that was observed directly from the field in relation to the time of the day.

Table 5-1 Summary of PC fluorescence measured at Pole 46 at different time intervals from the time of acquisition used as inputs in the multivariate regression model.

Day	Time of acquisition(09:30 GMT)		Minutes			
			-10 to +10	- 30 to +30	-60 to +60	PC daily
23rd	3035	Mean	3347.67	4326.43	4233.38	4027.37
		Median	3081	4313	4152	920.06
		Std Dev.	502.24	1057.67	798.43	3927
25th	2300	Mean	2324.71	2490.71	2443.38	2851.47
		Median	2300	2528	2479	554.72
		Std Dev.	192.19	204.75	211.05	2676
28th	3576	Mean	3588.67	3772.86	3681.23	3830.09
		Median	3576	3723	3576	343.30
		Std Dev.	370.16	371.20	370.13	3861

Table 5-1 above is a statistical summary of the PC fluorescence acquired of the individual days of the field campaign. This table represents the daily PC recorded at pole 46. They were used as part of the calculations of band ratios needed for the multivariate regression model in obtaining the model coefficients.

Table 5-2. Statistical summary of daily PC for the three field campaign days

Dataset	Minimum (RFU)	Maximum (RFU)	Median (RFU)	Mean (RFU)	Standard Deviation (RFU)
23rd September	2377	6699	3927	4038	920
25th September	2146	4615	2676	2851	554
28th September	3209	4658	3861	3830	343

A Statistical summary of the PC Fluorescence is shown in the table above in RFU as the unit of measure. The variation exhibited in the PC Fluorescence as indicated in figure 5-1 were attributed to several factors. The main factor that accounts for this variation was the amount of solar radiation reaching the surface of the Lake (Chawira, 2012; Häder et al., 1997). At various times of the day, different amounts of solar radiation reach the surface of the water. Another factor causing the fluctuation is the amount of cloud cover (Medina-Cobo et al., 2014). As indicated earlier, the first two days of field measurements were characterised by cloudy conditions. Which from figure 5.1 shows high variations whiles the measurement from the third day is relatively stable with peak measurements in the morning and evening. This is attributed to the effects of photoinhibition (Adir et al., 2003; Kurzbaum et al., 2007; Paul, 2001).

5.2. Wisp data

Wisp data compresses of three independent variables thus depending on the date the measurements were taken, 23rd, 25th and 28th respectively. These data were used to calculate the remote sensing reflectance (R_{rs}), these R_{rs} data was further convolved to match the spectra of the multispectral instruments.

As a result of lack of supplementary data, some sites were dropped and a total of 20 sites were used for further processing and analyses. A list of the selected sites with supplementary data is shown in the Table 5-3 below.

Table 5-3. List of sampled points

Point	Date	Latitude (DD)	Longitude (DD)	Time (GMT)
P1	23/09/2011	52.78606	5.31159	11:10
P2		52.79768	5.31225	11:18
P3		52.81106	5.31506	11:22
P4		52.82641	5.31992	11:29
P5		52.84235	5.32773	11:34
P1	25/09/2011	52.72663	5.31195	12:53
P2		52.75067	5.31291	12:59
P3		52.76459	5.31124	13:04
P4		52.77754	5.31075	13:09
P5		52.79201	5.31117	13:14
P6		52.80566	5.30754	13:19

P7		52.83618	5.30931	13:31
P8		52.84887	5.31581	13:36
P9		52.71702	5.30897	13:42
P1	28/09/2011	52.86424	5.14974	11:38
P2		52.88106	5.13437	12:38
P3		52.88112	5.13433	12:40
P4		52.88037	5.13397	12:54
P5		52.87196	5.14295	13:24
P6		52.86682	5.14799	13:44

Source: Field work from Chawira, (2012)

5.2.1. WISP Rrs (λ)

WISP-3 data from the field were processed and reflectance calculated from this data. Figure 5-2 below represents a total of all the three days of field campaign that was carried out on the IJsselmeer. The figure shows a plot of wavelength against surface reflectance.

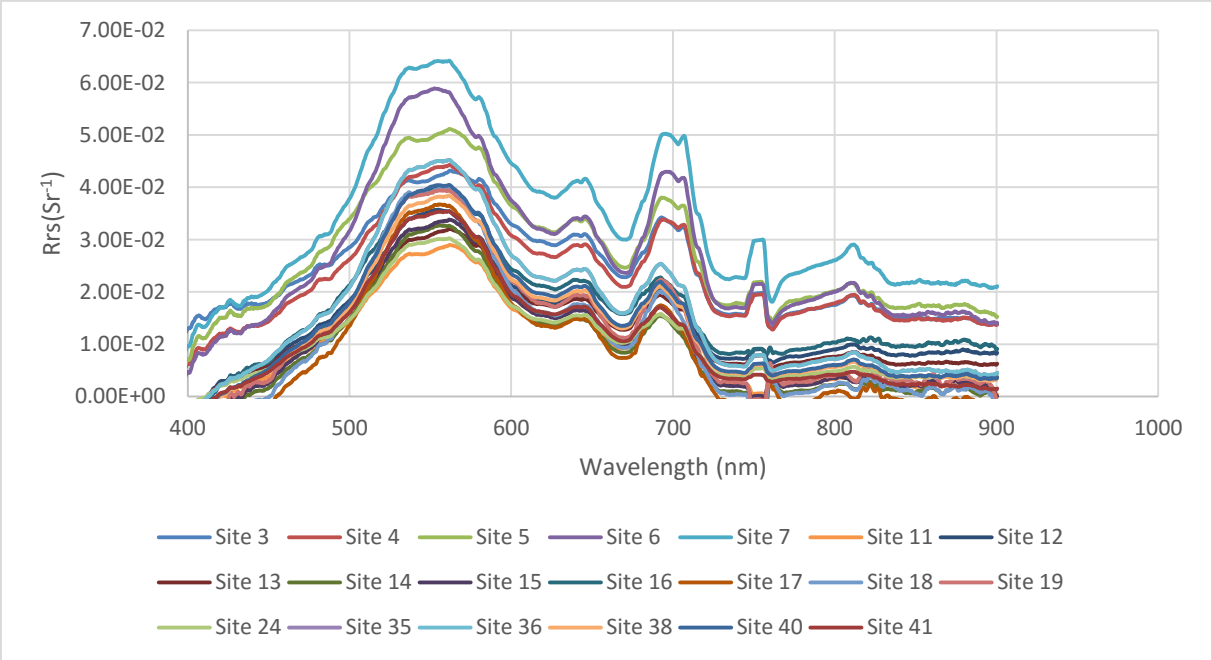

Figure 5-2 A summary of all valid field measurement carried out on the IJsselmeer used for further processing in this research.

For the generated spectra, the coefficient of variation (CV) was calculated for the spectra as shown below in the figure with a bold thick black line. The specific absorption and scattering of water molecules properties of each optical spectra given as a function of wavelength in relation to light is shown in the figure.

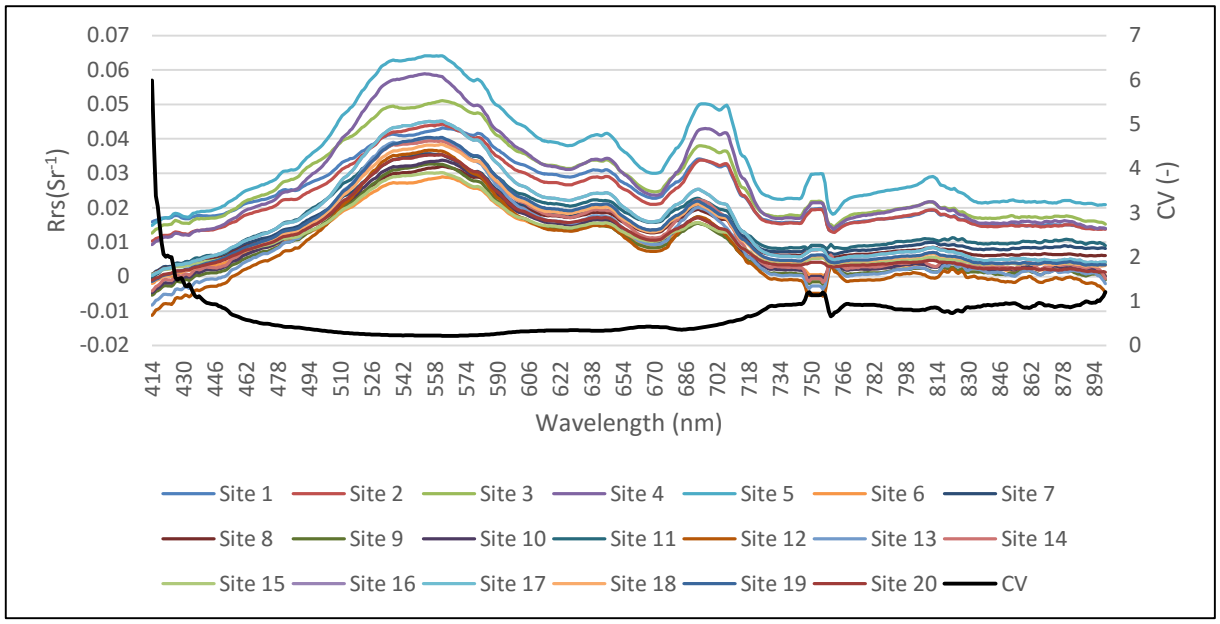

Figure 5-3 Coefficient of variation (CV) for all valid spectra on the IJsselmeer.

So with cloudy conditions on days field campaign were conducted, and with the assumption that absorption peak of PC in the lake is around 670 nm with all other conditions remaining constant for the lake, the coefficient of variation for the maximum level of uncertainty was approximated at 0.422.

5.2.2. Calibration and Validation of Selected models

The semi-empirical models selected for this research were calibrated and validated with in-situ measurement. As described in section 4.5, a multivariate regression was performed. This regression included, PC measured as the independent variables and band ratios obtained from the available bands for prediction of PC in the various multispectral instruments as dependent variables. This regression model came out with model coefficients that were needed for estimating PC using the selected semi-empirical model.

5.2.2.1. In-situ Measurement

In-situ PC were obtained from pole 46 and 47 as noted in section 3.2.1.2. This data was measured at fixed location with a YSI probe every 10 minutes daily. But for the purposes of this research not all data obtained from these poles were used. Data used in this research was limited to 8:00 GMT to 15 hours GMT. This period was chosen to account for the peaks periods the lake is in used as a recreational and socio-economic resource (Evans, 1999; Santamaria-del-Angel et al., 2011).

5.2.2.2. Band ratios

Various band ratios were used depending on the model. For Sun et al. (2015), 10 band ratios were required for Estimating PC whiles Vincent et al. (2004) required 6 band ratios originally. But once there were some differences regarding the wavelengths needed for this calibration, the model was recalibrated with 4 band ratios.

Table 5-4 Band ratio for the selected models

Sun et al. model	Vincent et al. model
Band 1	Band 3 by Band 1
Band 2	Band 4 by Band 1
Band 3	Band 4 by Band 3

Band 4	Band 5 by Band 3
Band 4 by Band 3	-
Band 4 by Band 2	-
Band 4 by Band 1	-
Band 3 by Band 2	-
Band 3 by Band 1	-
Band 2 by Band 1	-

5.2.2.3. Calibration and Validation of Models

Before calibrating the models (that of Sun and Vincent) we investigated their validity through direct application of the model on observed radiometric data and compered the outcome to the measured PC. (Fig. 5-4) shows the results obtained from the original models of Sun et al., (2015)(Fig5-4-a) and Vincent et al.,(2004) versus the measured values of PC.

(a) (b)

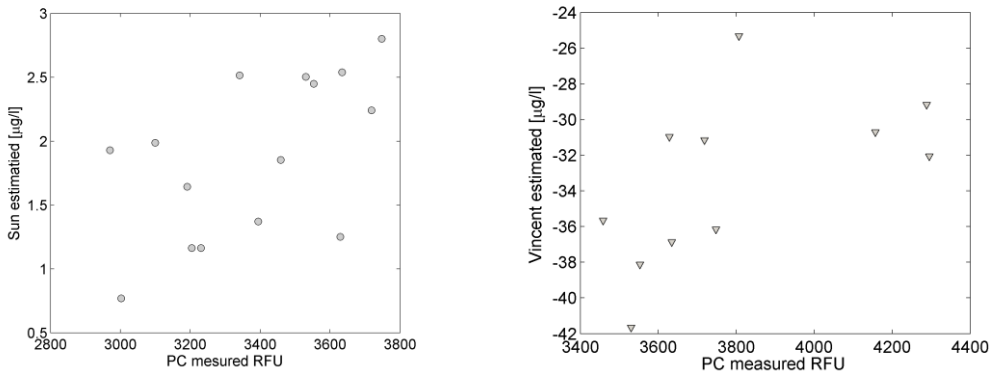

Figure 5-4 Estimated versus measured PC sing original models of Sun et al., (2015) (a) and Vincent et al. (2004), (b).

From the test calibration conducted with the original Sun model, for PC values less than 3800 RFU an R^2 is 0.32 was obtained and there was no correspondence with in-situ measured PC and estimated as in-situ measured were in RFU while Sun was in µg/l. The model was done adopted to convert them into the same unit for assessment. When this applied on the Vincent model R^2 of 0.32 was obtained. Vincent model worked for PC values above 3400 RFU.

The in-situ measured PC from the sampled sites were ordered and divided into two set. One for calibration and the other for validation. The second set of data which was made up of the eleven (11) elements was used as calibration set whiles the first set which consisted of 9 out of the twenty was used for Validation. Below in Table 5-5 and 5-6 are the summary of the calibration and the validation sets and the coefficients from the model by Sun et al. (2015), these coefficients were used in estimating PC.

Table 5-5 Summary of calibration and validation datasets

	Minimum (RFU)	**Maximum (RFU)**	**Mean (RFU)**	**Standard deviation (RFU)**

Calibration	3530.667	4307	3878.97	316.113
Validation	2970.33	3458.667	3210.19	168.392

Table 5-6. Coefficients generated from a multivariate regression of Sun et al Model.

Coefficients	**Landsat 8 OLI**	**Sentinel-2 MSI**
K_0	0	0
K_1	9580416	257950.2
K_2	2272241	217611.2
K_3	-110713	-422459
K_4	-5789177	9091.518
K_5	-557160	-27071.9
K_6	308431.6	-2409.89
K_7	-4243.26	228.6008
K_8	-39330.1	6566.786
K_9	-9415.57	920.7541
K_{10}	35717.49	-842.775
R^2	0.6993	0.5255

These coefficients were obtained from the regression model performed on the dataset. The fitting constant of the regression model was set to Zero which is indicated here by K_0 and K_1 to K_{10} represents coefficients for the 10 independent variables. As shown in Table 5-6 above. This process was repeated for Sentinel-2 MSI as well.

After the regression model was performed, coefficients from the regression model were used to predict the modelled PC. Both had positive r^2 as shown in the figures below.

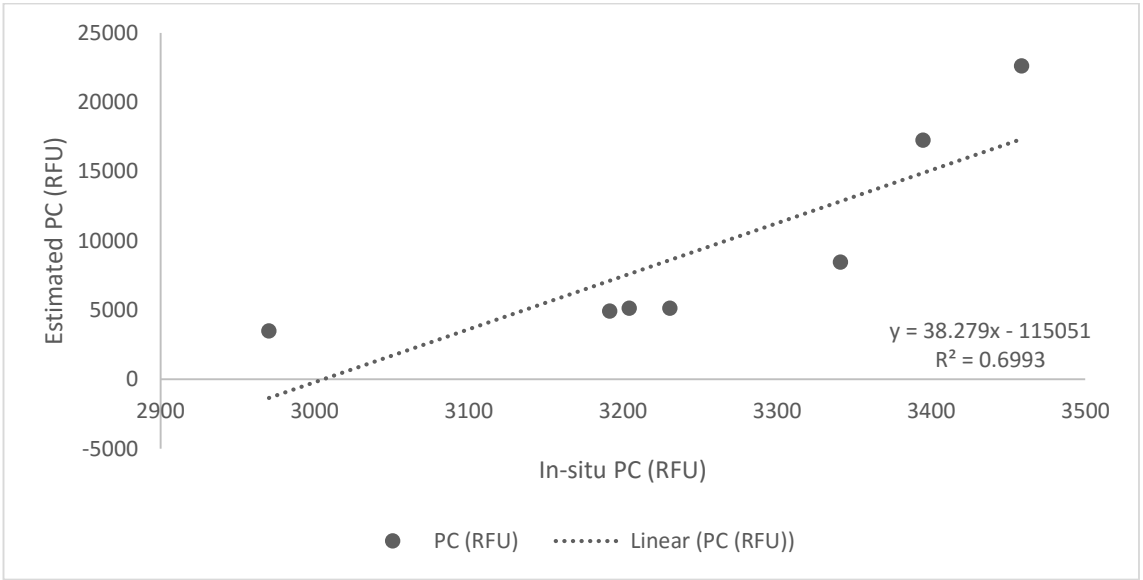

Figure 5-5 Validation of in-situ measured PC and estimated PC of Sun model for Landsat 8 OLI

Data from sentinel-2 MSI were calibrated and validated as well. The following figure is a representation of the validation of the sun model on sentinel-2 MSI sensor.

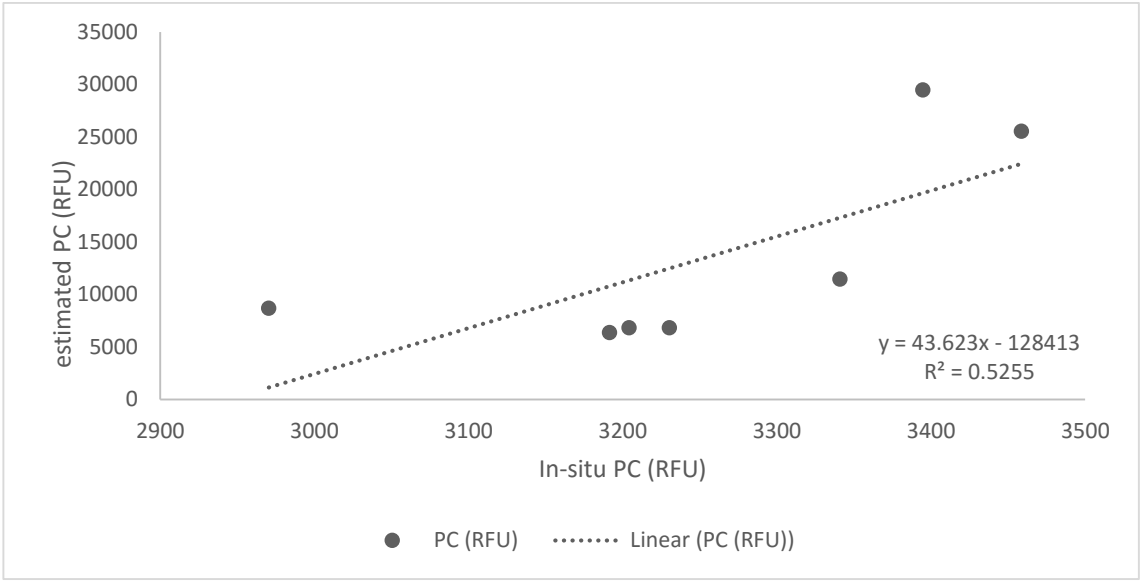

Figure 5-6 Validation of in-situ PC with estimated PC for Sun model on Sentinel-2 MSI

A linear regression model was performed for Vincent et al. (2004) model. Based on the band ratios for the model, five coefficients were generated. The table below shows the coefficients for both Landsat 8 OLI and Sentinel-2 MSI.

Table 5-7. Coefficients generated from multivariate regression model for Vincent et al model.

Band ratios	Landsat 8 OLI	Sentinel-2 MSI
K_0	0	0
K_1	1100.092	-920.757
K_2	-1385.7	3589.534
K_3	6351.115	3385.88
K_4	-2984.71	-238.415
R^2	0.5343	0.0319

Out of the sum, 60% of the data was used for calibration and 40% used for validation. Results obtained from the calibration and Validation of this model, Vincent et al., (2004), is present below in the following figure.

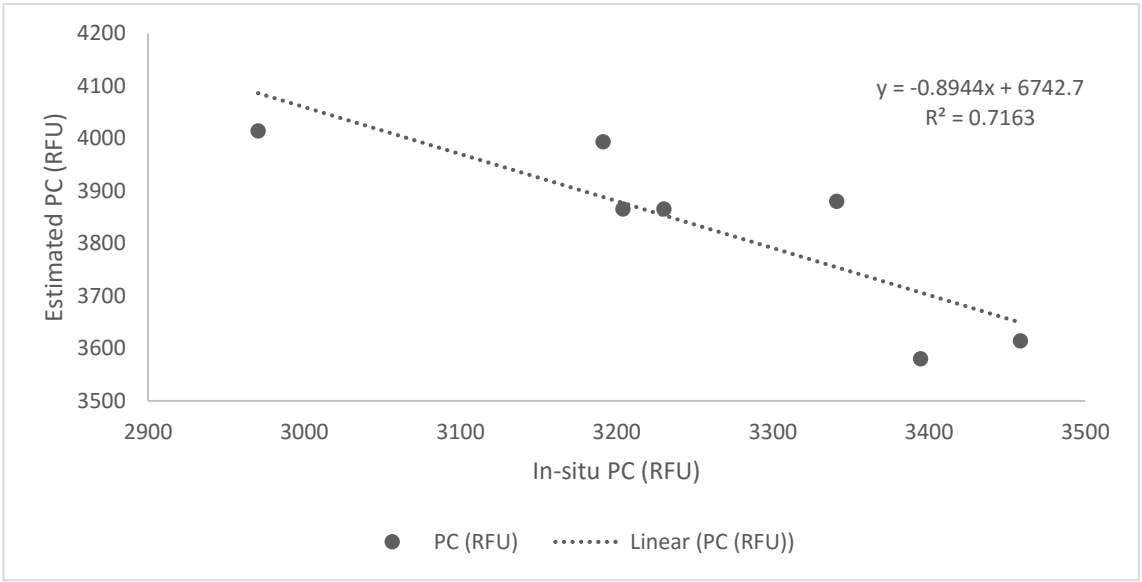

Figure 5-7. Validation of Vincent model for Landsat 8 OLI.

The model application on Sentinel-2 MSI did not produce good results. The model prediction did not correlate well with the in-situ measurement. The reason for this poor correlation could be attributed to several factors. One is that, the model was designed for Landsat thematic mapper and therefore did not consider the band 2, for Sentinel-2, known as the blue band but rather takes into consideration the ultra-blue bands also known as the coastal aerosol band.

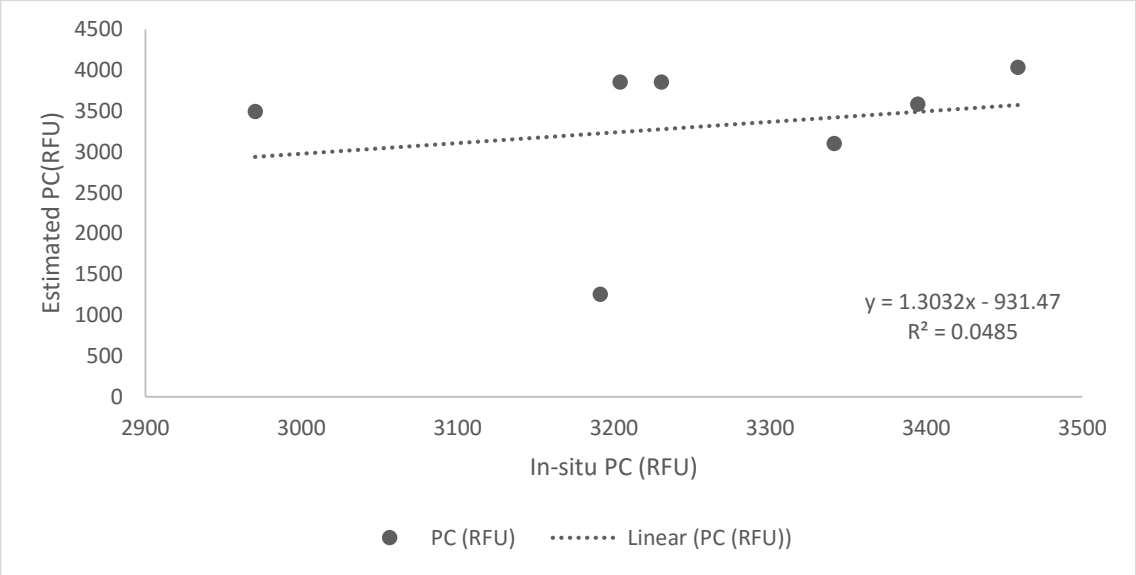

Figure 5-8 Validation of Vincent model for Sentinel-2 MSI

Figure 5-8 above is a validation of the model. It was observed that, the model did not performance as much as Sun model did. But, the model had a positive coefficient of correlation (R2) of 0.3584. Below in Table 5-7 is a summary of the validation of the model calibration.

Table 5-8 Summary of validation of model calibration

	Landsat 8 OLI		**Sentinel-2 MSI**	
	Sun model	Vincent model	Sun model	Vincent model
RMSE	9228.058	646.51	13651.64	866.34
MAPE (%)	186.72	18.11	309.88	21.04
R^2	0.6993	0.7163	0.6572	0.0485

The results obtained from the validation of the models as shown in Table 5-7 above suggest that Sun model performed better in estimating r2 but for the other factors like MAPE and RMSE it did not do well. For Sun et al. model, MAPE and RMSE of 186.72 % and 309.88 % respectively were obtained for both sensors. The model in this case is said to have over fitted the training data (calibration set) producing a good r2 of 0.6993 while the other parameters considered thus MAPE and RMSE are too high. For this reason the Vincent model was adopted for this research work with r2 of 0.7163 and 0.0485 for Landsat 8 OLI and Sentinel-2 MSI respectively.

Below in Figure 5-8 is a comparison of the similarities between the bands used for the estimation of PC.

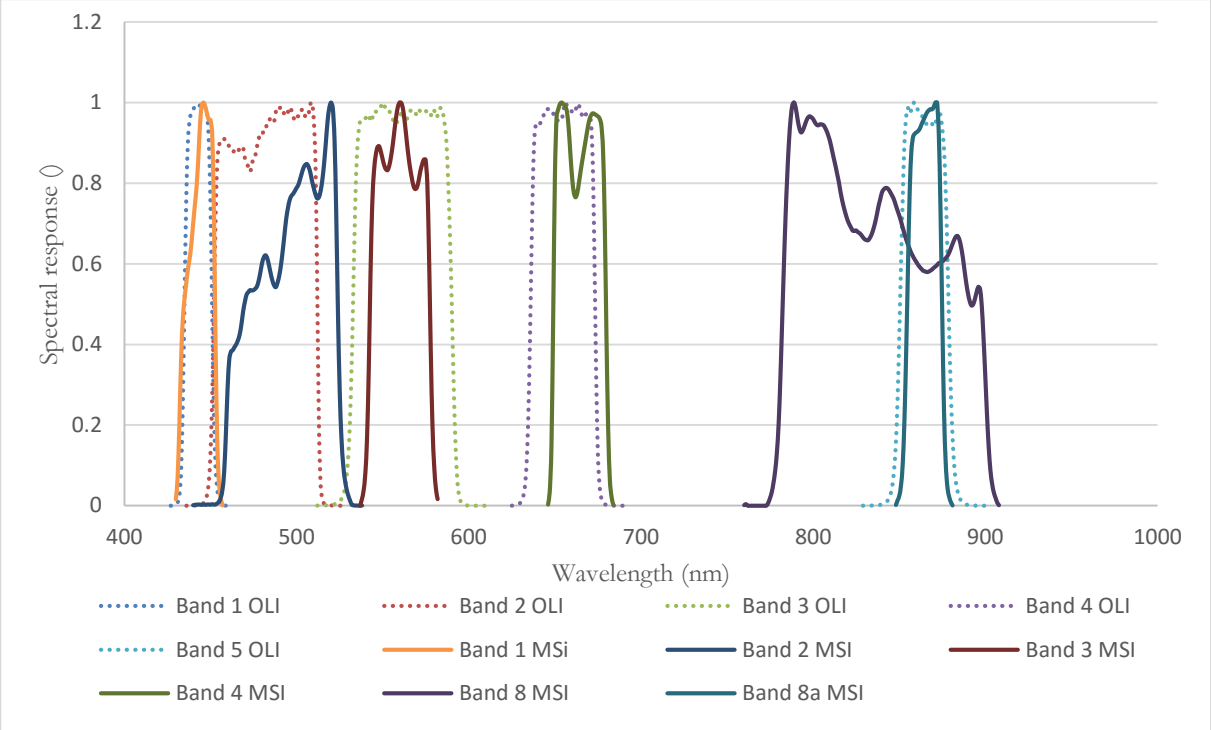

Figure 5-9. Band similarity comparison between Landsat 8 OLI and Sentinel-2 MSI visible and near infrared bands

5.3. Convolving of remote sensing reflectance to Landsat 8 OLI

Wisp data was interpolated to fit Landsat 8 OLI and Sentinel-2 MSI spectra. The interpolation was performed to normalize the spectral range of the two sensors to a 1 nm range. Therefore the interpolation took into consideration the minimum and maximum of various wavelengths to come out with a central wavelength that was representative of the total bandwidth. The results of this interpolation are displayed in Table 5-9 below.

Table 5-9. Summary of wavelength used for convolution and their sum of the convolved spectra

Bands	Wavelength Range (nm)		Central Wavelength (nm)	Computed SRF (-)
Coastal Aerosol	427	459	443	0.6945
Blue	436	528	482	0.9624
Green	512	610	561	1.5111
Red	625	691	658	1.2888
NIR	829	900	864.5	0.6776

Table 5-9 below shows the results of convolution as summarized by day of measurement.

Table 5-10. Convolved WISP-3 reflectance data with simulated Landsat 8 OLI spectra

Bands	Summary of selected sites (R0-(-))		
	23rd September 2011	25th September 2011	28th September 2011
Band 1	0.036812	0.021093	0.022913

Band 2	0.044226	0.027843	0.030696
Band 3	0.051285	0.034733	0.038497
Band 4	0.045471	0.028824	0.032334
Band 5	0.030308	0.014811	0.017336

It was observed that the various days had different reflectance curves which could be attributed to weather condition on those various days. As discussed in section 3.2.1, the first day was characterised by cloudy conditions. For Sentinel-2 MSI, the following results were obtained after convolution was performed.

Table 5-11. Mean convolved WISP with Sentinel-2 MSI

Bands	**Summary of selected sites (R0-(-))**		
	23rd September 2011	25th September 2011	28th September 2011
Band 1	0.01642	0.002433	0.004722
Band 2	0.031928	0.016788	0.018724
Band 3	0.050681	0.03412	0.037832
Band 4	0.027378	0.012725	0.015274
Band 8a	0.03782	0.015378	0.017425

5.4. Atmospheric correction

5.4.1. Landsat 8 OLI correction

The application of equations 9 and 10 in section 4 of this work results in atmospherically corrected images. The images were first converted from TIFF to BIL format, making them compatible with ENVI processing. This process was performed by taking into considering FLAASH default setting and using only the multispectral bands of Landsat 8 OLI. In processing the images, the scale factor was set to single scale factor for all bands that were used in processing to 1.000. The mid-latitude summer atmospheric model was used considering the date of image acquisition of the first two images while mid latitude winter for the image of 14th March 2016. Maritime was selected as the aerosol model.

After all the necessary information were inputted from the image metadata, the atmospheric correction was performed. This produced atmospherically corrected images with reflectance data. The following equation was used to normalise the reflectance values within the range of 0 and 1.

$$((B1 < 0)*0 + (B1 > 10000)*1 + (B1 > 0 \text{ and } B1 < 10000)*\text{float}(b1))/10000 \quad \text{Equation 14}$$

Where, if the pixel value is less than or equal to zero (0) it is multiplied by 0 and if the pixel greater than or equal to 10000 it is multiplied by 1, if the pixel value is greater than 0 and less than 10000 it is multiplied by its floating value and the result is divided by 10000.

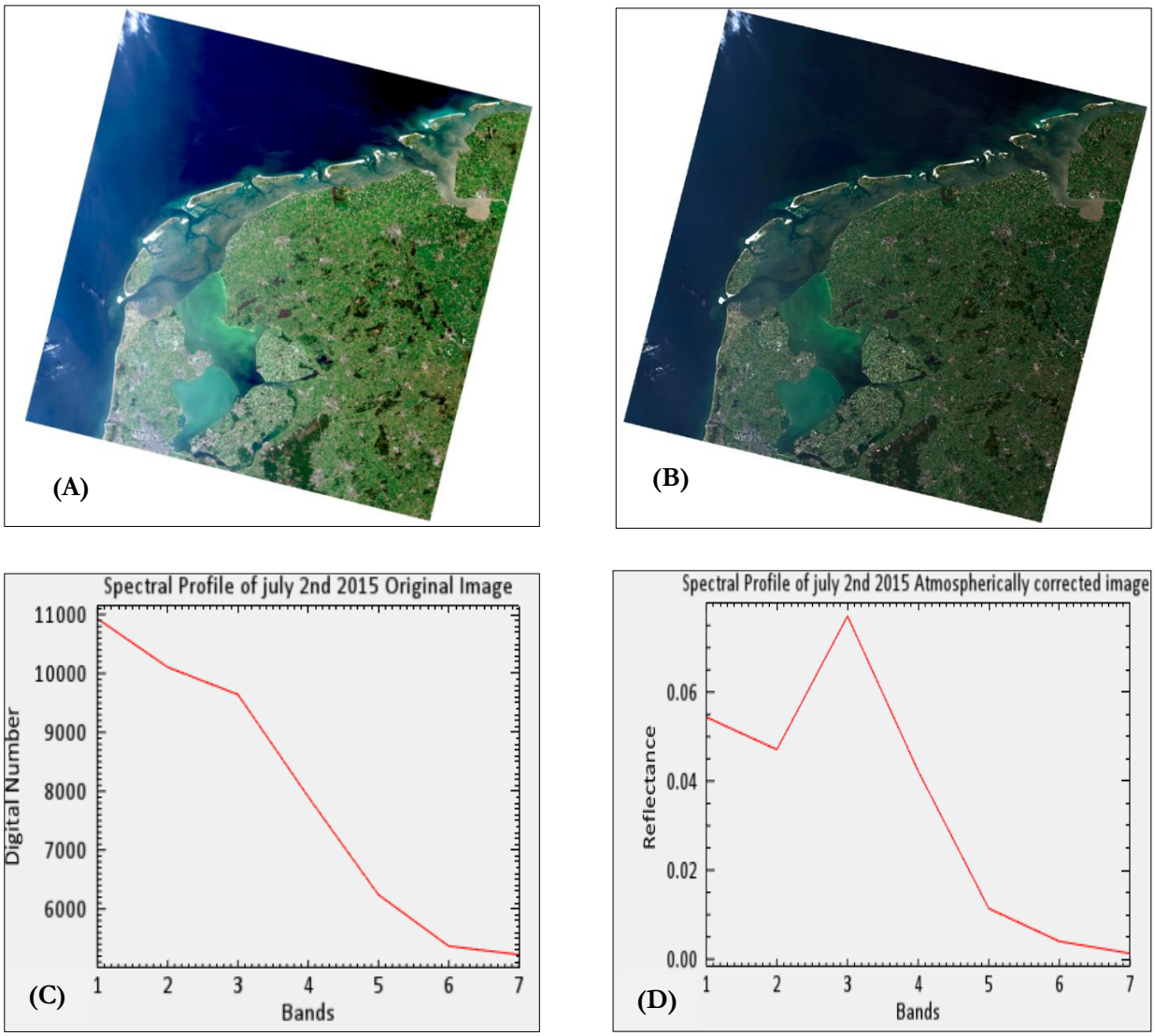

Figure 5-10 Original image of July 2nd is shown in figure (A). Figure (B) is the Atmospherically Corrected image (C) is the Spectral profile of the Original image and Figure (D) is the Spectral profile of the atmospherically corrected image

5.4.1.1. Verification of the Landsat 8 OLI Images

The accuracy of FLAASH atmospheric correction was evaluated by comparing the derived atmospheric corrected water leaving reflectance from an image of 2nd July 2015 and convolved WISP-3 data obtained from the field to Landsat spectra. For each site, a comparison is made between the convolved WISP-3 data with satellite image obtained on the 2nd of July 2015.

Considering the launched period of Landsat 8 and the date of field campaign, there could be other atmospheric conditions that affected the measured in-situ data that Landsat 8 did not take into consideration. For instance the effects of neighbouring substances like detritus, surface white caps among others creating adjacency effects (Hunter et al., 2010; T. Lee & Kaufman, 1986).

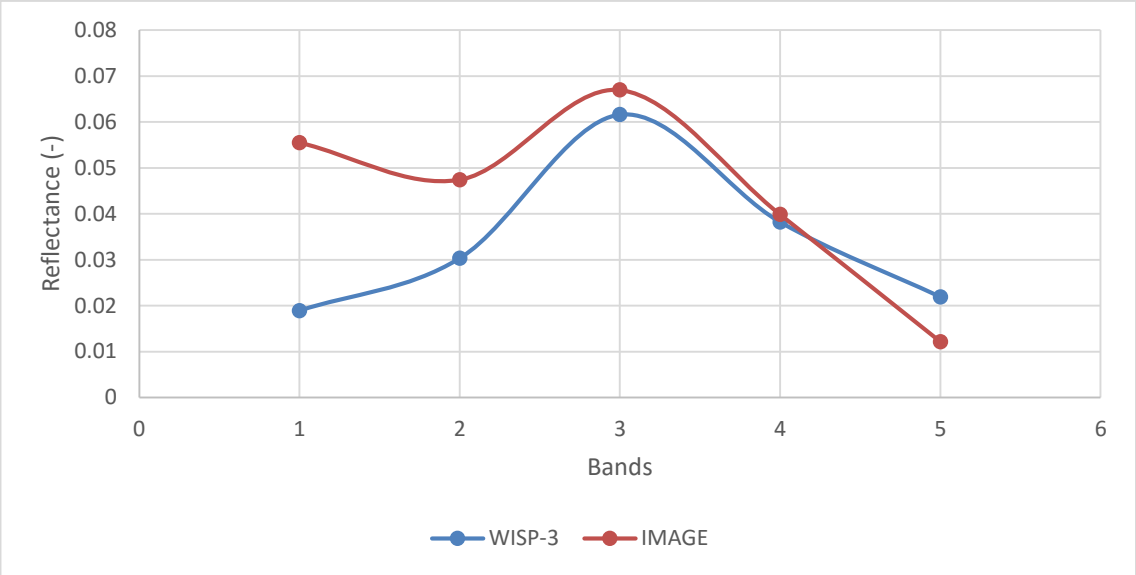

Figure 5-11 An example of the accuracy assessment of atmospheric correction on the image obtained on the 2nd of July 2045 with convolved WISP-3 Reflectance for site 5.

5.5. Application of selected model on Landsat 8 OLI images

The results from the calibration and validation of the model indicate that the (Vincent et al., 2004) was the best model for this particular case. Therefore, it was applied on the satellite images of Landsat 8 OLI.

The application process is briefly described below in Figure 5-12.

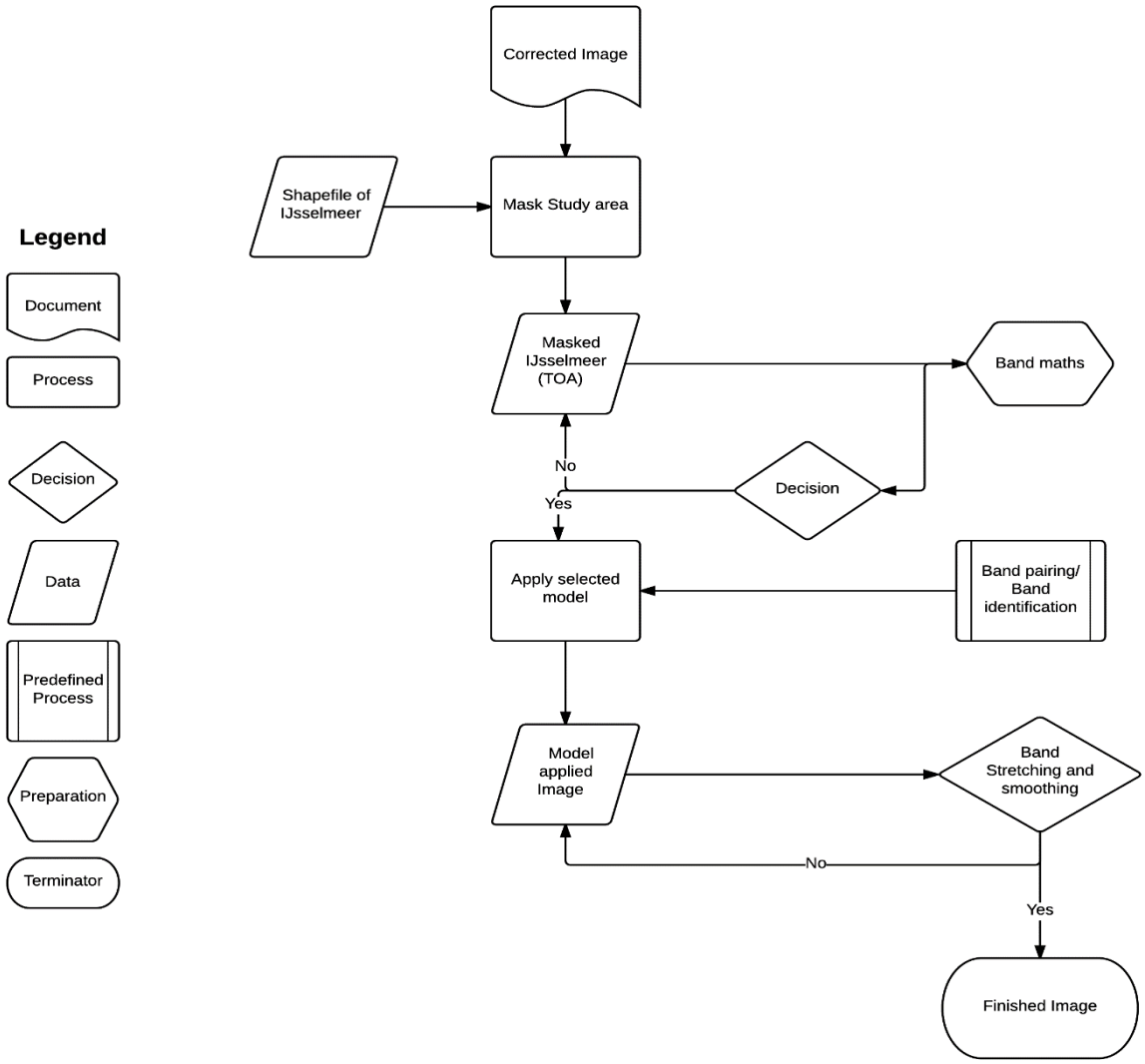

Figure 5-12. Model application flowchart

5.5.1. Application of Model

5.5.1.1. Recalibrated Sun et al model on Landsat 8 OLI

The application process was performed using ENVI 5.3. The satellite images obtained for the various days were processed and the study area was masked out of the complete image. The masked images of the study area were then classified with the band maths tool in ENVI. The selected model equation with the coefficients calculated was inputted into equation 8 and the appropriate bands selected. As noted in Table 5-4 and 5-7 for Vincent model.

In Figure 5-12 below is Landsat 8 OLI images of the study area for July 2nd. September 17th and 14th of March 2016 followed in the next figure respectively. The image of July showed PC blooms in the IJsselmeer (Chawira, 2012; Simis et al., 2005). The bloom is attributed to favourable weather conditions, good temperature, light intensity among others factors. These factors are further supported by the work done by Kanoshina et al. (2003) in the Gulf of Finland, which states that natural phenomenon like global warming and wind direction significantly affects the spatial distribution of cyanobacteria than the vertical transportation of nutrient.

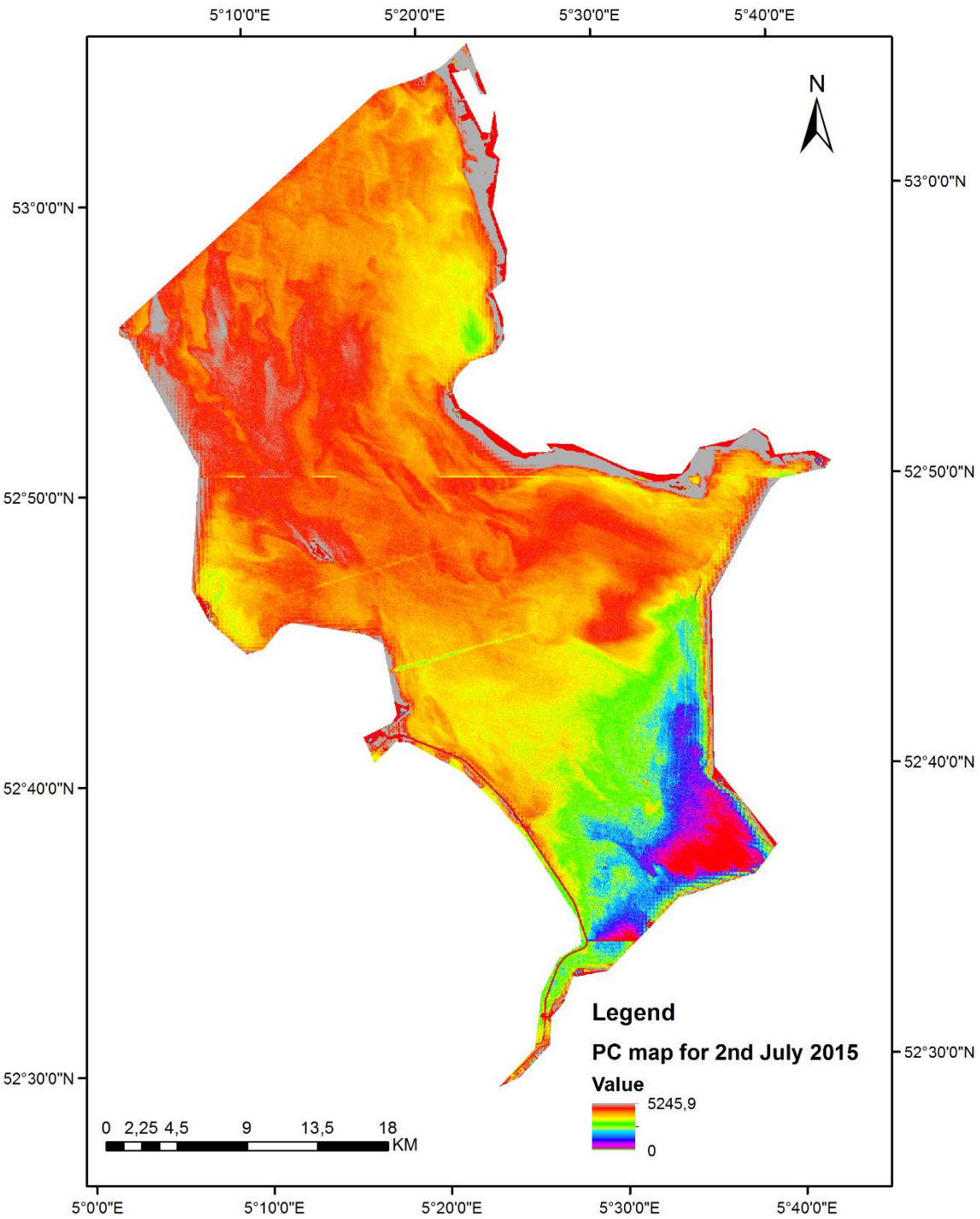

Figure 5-13. Map of PC obtained from Landsat 8 OLI image of 2nd July 2015 of the Study area.

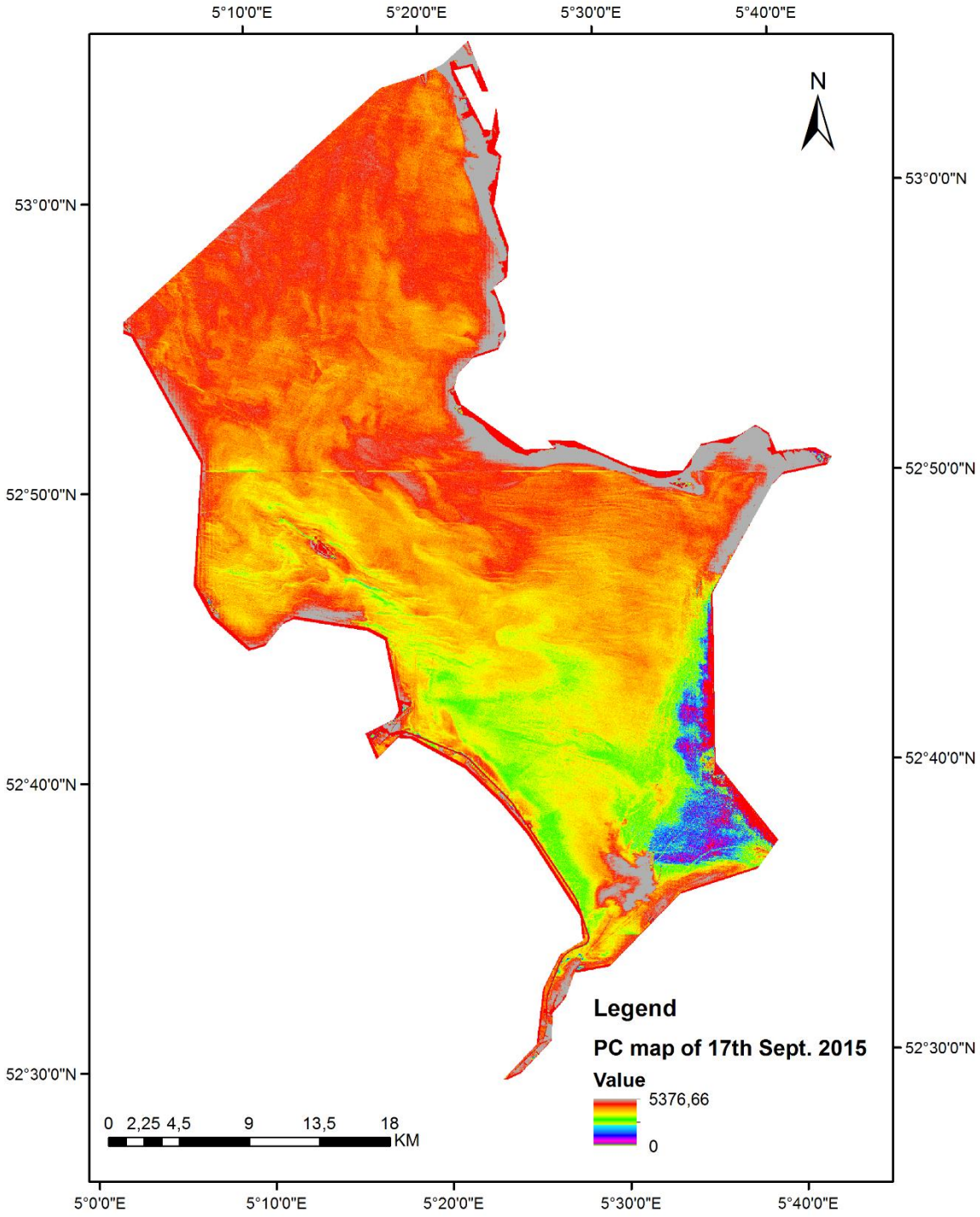

Figure 5-14 Map of PC derived from Landsat 8 OLI image of 17th September, 2015

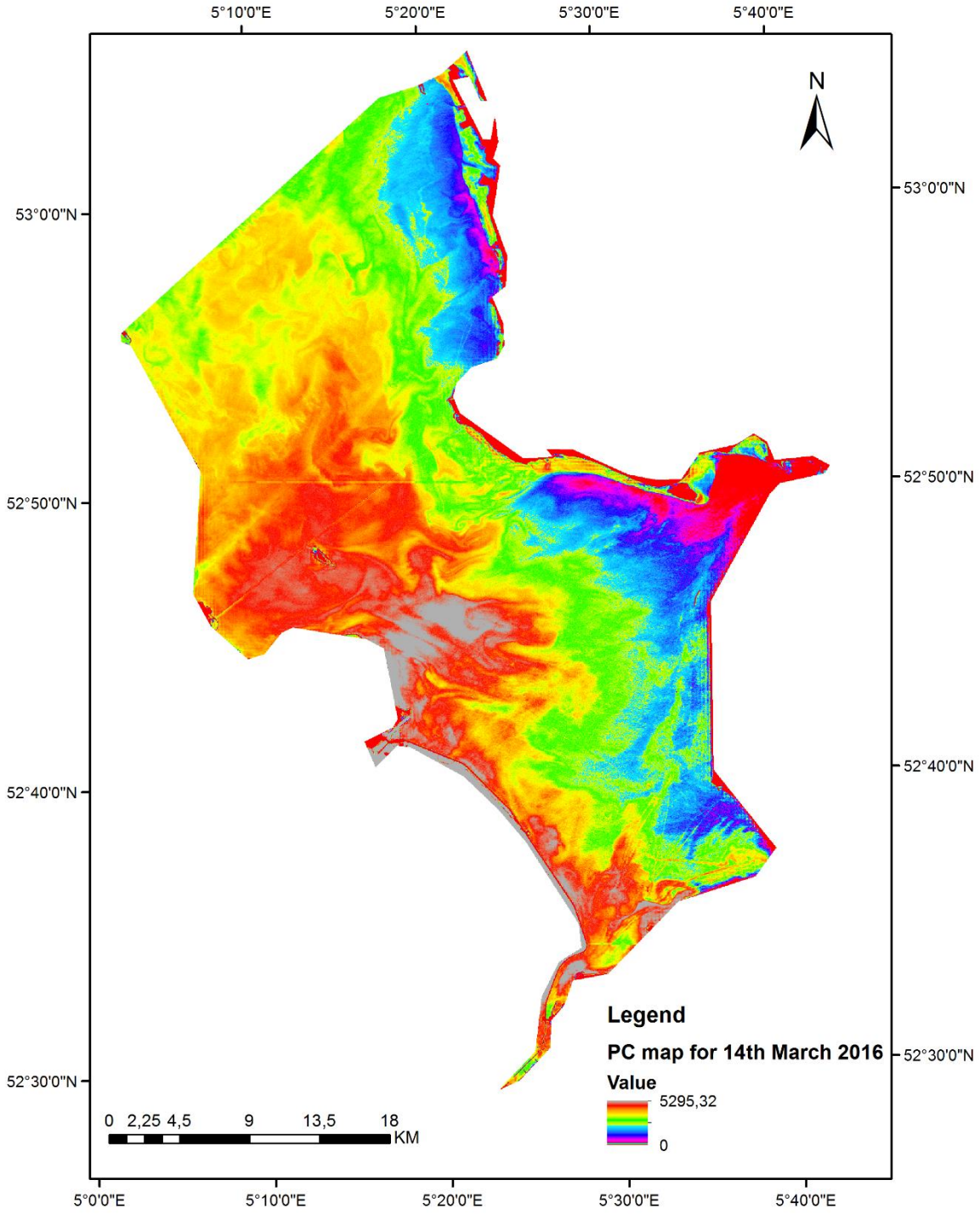

Figure 5-15. Map of PC derived from Landsat 8 OLI image of 14th March 2016.

The application of the model on a second image obtained on the 17th of September, 2011 showed a similar trend of the development of PC. Based on wind movement and trend over the study area it has been observed that there is a general circulation of the wind in the study area (windfinder, 2016). The period was found to be synonymous with the bloom season of cyanobacteria. This trend is an affirmation of the growth pattern of PC reducing in quantity from summer with suitable weather conditions through into winter with little PC in the lake.

After the PC maps were generated, the sampled sites from which in-situ data were measured were overlaid on the maps. This process was used to obtain PC values for the sampled sites. The results obtained thereafter did not correlate well. The reason behind this poor correlation was largely due the temporal variation between the two datasets used. In-situ measured PC were obtained in September of 2011 while satellite images were from July and September 2015.

The model was applied to a third image for 14th march 2016. This image shows the reduction in PC levels in the lake. The reason being unfavourable weather pattern thus with decreasing temperatures, low amount of sunlight among others. The image shows signs of PC on the upper left (North – western) part of the image. This might not necessarily be PC as that can be attributed to some clouds. The image was said to be about 23.3 % cloudy. Therefore not all clouds were completely removed by the atmospheric correction method.

5.6. Sensitivity analysis

Sensitivity analysis could not be carried out. This pertains to the factor that the data collected on site during the field work and those generated from the multispectral instrument are spatial-temporal not compatible. Data for the field were obtained in 2011 while satellite images are from 2015 and 2016.

6. CONCLUSION AND RECOMMENDATION

6.1. Conclusion

This research was aimed at assessing two semi-empirical band ratio models (Sun et al. (2015) and Vincent et al. (2004)) for estimating cyanobacteria (PC) and to assess the applicability of the best model on multispectral sensors. To achieve these goals some questions were asked.

1. Can we deduce useful information from multispectral analysis of cyanobacteria?
2. What is the accuracy of derived cyanobacteria products from Landsat 8 OLI and Sentinel-2 MSI?
3. How do cyanobacteria vary at fine spatial scale?

The following chapter presences the findings to these questions and recommended solutions to problems not addressed. Each specific research question was assessed in a subsection of this chapter as shown below.

1. Deduction of useful information.
2. The accuracy of derived PC.
3. Verification of cyanobacteria at finer scale.

On a much larger scale, the sensors used in this work all have their setbacks when it comes to the estimation of PC and other water quality variables and or in other fields of study. These setbacks ranged from spatial resolution, revisit time, signal to noise ratio, pixel size, availability of good satellite data etc.

To comprehensively compare the performance of different sensor with these kinds of setbacks, attention was placed on the individual strength and weakness of these sensors.

6.1.1. Deduction of useful information

The diversity of remotely sensed cyanobacteria is characterised by the sensor properties. These properties generate different types of data with different importance per the analysis conducted. During the cause of this research work, it observed that the Sun model overfitted the data used in it calibration and validation thereby producing a higher r^2 than the Vincent model. When other accuracy assessment variables like RMSE and MAPE were compared the model of Vincent proved to be more reliable. More details of this assessment are presented section 6.2.2 below.

The findings further showed that, Vincent model though was not designed for Landsat 8 OLI, but with some few modification was able to estimated PC. The modelled results here also showed that there are other factors that may have caused the variation particularly in the satellite images. For instance, the presence of chlorophyll in the lake, the seasonality of PC and other algae could also affect the findings as shown in the images.

The results for the application of the model on the images showed that wind condition, nutrients, sunlight and the right amount of temperature proved to be very important in the distribution of PC. The lack of the absorption band for PC at around wavelength 620 nm.

The findings of research work by Wheeler et al. (2012) states that, for effective monitoring of cyanobacteria by water resource managers, it is prudent to consider spatial, spectral, temporal and atmospheric conditions in their analysis. This according to him would help improve the health risk management. The findings of these research support the factor that spatial-temporal variation is a critical aspect of water quality management.

6.1.2. The Accuracy of derived PC

The accuracy of the maps generated hereafter have to be taken with caution as the models state here still have to undergo validation. There was a poor correlation could be attributed WISP-3 measurement but further investigation is needed to find the cause of this poor correlation.

Results obtained from section 5.2.2.3, which deals with the model calibration and validation using in-situ measurement as independent variables for validation showed that the model of Vincent was a much better

model when compared with the model of Sun et al. Sun model was observed to have over fitted the datasets but other accuracy assessment parameters indicated the model was not accurate enough to be used for this work.
Hodoki et al. (2011) explained in their work the importance of time in the variation of cyanobacteria. Which was factored in during the cause of this research work. In order to make a comparison of two datasets it would be advisable to obtain field measurement and satellite images close to one another for easy and accurate validation and or comparison. For a better estimation of PC with the use of these models, hyperspectral date would be needed.

6.1.3. Variation of cyanobacteria at a finer scale.

Previous researches conducted on the use of remote sensing in detection and monitoring of cyanobacteria indicates that at higher resolutions the accuracy of detecting cyanobacteria is high (Gons, 2004; Simis et al., 2005; Wheeler et al., 2012). The use of these multispectral sensors therefore was assumed to have a high level of accuracy. The spectral and spatial properties of these multispectral sensors as compared to other sensors used in the past are very high (Palmer et al., 2015) and therefore they were expected to produce PC map at a fine scale. This was not the case as the direct applicability of the best model here (Vincent model) what not feasible for Sentinel-2 MSI. The multispectral instruments used in this research lacked the 620 nm band for accuracy assessment of PC. According to Palmer et al. (2015) past sensors such as MERIS which had over 10 years of satellite data archive and a spatial resolution of 300 meters made it a valuable resource for water quality monitoring. Section 3.2.2. on the satellite data, provides details of the current ocean colour sensors used in this work.
Unfortunately, the application of selected model on Sentinel-2 was not completed though an attempt was made at estimating PC. Therefore, the research question on the variation of cyanobacteria at fine scale was not answered.

6.2. Recommendation

The potential of using Sentinel-2 for water quality monitoring is very high. This research has shown that in the multivariate regression model that was used in obtaining the model coefficients for PC estimation using the model proposed by Vincent (2015). This potential needs to be investigated further by applying the said model on Sentinel-2 MSI images. This was the major limitation of this MSc research work. Some recommendation arrived at included:

- Field measurement should cover about 60 percent of the study area. This will allow for a better understanding of the processing taking place in the lake.
- It was further observed that though the model attempted estimated PC, there is the need for further work to be done with recent field measurement to go along with satellite images (hyperspectral data). Lack of recent field measurement could resulted in a poor correlation between the two datasets used for this work.
- Regarding the application of the model on Landsat 8 OLI, which is sensitive wavelength selection. The correct wavelengths and or bands are to be selected or this could lead to an overestimation or underestimation of PC.
- Atmospheric correction must be given a lot of attention in order to estimate PC accurately. Therefore accurate atmospheric correction would have to be applied to the images before the model is applied.
- Wind influence was a major factor that affected the distribution of PC in the lake. In future, it is recommended that wind influence is investigated fully.
- It is recommended that for any kind of comparison is to be made using the results produced in this work more validation would be needed.

LIST OF REFERENCES

Adir, N., Zer, H., Shochat, S., & Ohad, I. (2003). Photoinhibition – a historical perspective ∗ . *Photosynthesis Research*, *76*(1-3), 343–370. http://doi.org/10.1023/A:1024969518145

Ahn, C.-Y., Joung, S.-H., Yoon, S.-K., & Oh, H.-M. (2007). Alternative alert system for cyanobacterial bloom, using phycocyanin as a level determinant. *Journal of Microbiology (Seoul, Korea)*, *45*(2), 98–104. Retrieved from http://www.ncbi.nlm.nih.gov/pubmed/17483793

Bartram, J., WC, C., I, C., J, J., & OM, S. (1999). Introduction, 1–14. Retrieved from https://www.researchgate.net/publication/253793906_Introduction

Berthelot, B., & Santer, R. (2009). *Recommendation for the calibration for Sentinels : S2 and S3* (Vol. 33). Retrieved from http://calvalportal.ceos.org/c/document_library/get_file?uuid=b10e77b2-4852-486a-81b2-0b04fe181e5f&groupId=10136

Brient, L., Lengronne, M., Bertrand, E., Rolland, D., Sipel, A., Steinmann, D., … Bormans, M. (2008). A phycocyanin probe as a tool for monitoring cyanobacteria in freshwater bodies. *Journal of Environmental Monitoring : JEM*, *10*(2), 248–255. http://doi.org/10.1039/b714238b

Chawira, M. (2012). *Monitoring blue-green algae in the IJsselmeer using remote sensing and in-situ measurements. Enschede, The Netherlands: University of Twente*. University of Twente. Retrieved from http://www.itc.nl/library/papers_2012/msc/wrem/chawira.pdf

Cheung, M. Y., Liang, S., & Lee, J. (2013). Toxin-producing cyanobacteria in freshwater: A review of the problems, impact on drinking water safety, and efforts for protecting public health. *Journal of Microbiology*, *51*(1), 1–10. http://doi.org/10.1007/s12275-013-2549-3

Codd, G., Bell, S., Kaya, K., Ward, C., Beattie, K., & Metcalf, J. (1999). Cyanobacterial toxins, exposure routes and human health. *European Journal of Phycology*, *34*(4), 405–415. http://doi.org/10.1080/09670269910001736462

Dash, P., Walker, N. D., Mishra, D. R., Hu, C., Pinckney, J. L., & D'Sa, E. J. (2011). Estimation of cyanobacterial pigments in a freshwater lake using OCM satellite data. *Remote Sensing of Environment*, *115*(12), 3409–3423. http://doi.org/10.1016/j.rse.2011.08.004

Dekker. (1993). *Detection of optical water quality parameters for eutrophic waters by high resolution remote sensing. Amsterdam: Vrije Universiteit*. Vrije Universiteit Amsterdam. Retrieved from http://dspace.ubvu.vu.nl/handle/1871/12714?show=full

Dekker, Malthus, T. J., & Seyhan, E. (1991). Quantitative modeling of inland water quality for high-resolution MSS systems. *IEEE Transactions on Geoscience and Remote Sensing*, *29*(1), 89–95. http://doi.org/10.1109/36.103296

Dekker, W. (2004). What caused the decline of the Lake IJsselmeer eel stock after 1960? *ICES Journal of Marine Science*, *61*(3), 394–404. http://doi.org/10.1016/j.icesjms.2004.01.003

Drusch, M., Del Bello, U., Carlier, S., Colin, O., Fernandez, V., Gascon, F., … Bargellini, P. (2012). Sentinel-2: ESA's Optical High-Resolution Mission for GMES Operational Services. *Remote Sensing of Environment*, *120*, 25–36. http://doi.org/10.1016/j.rse.2011.11.026

ESA. (2006). MERIS Product Handbook. *October*, (2), 130. Retrieved from https://earth.esa.int/pub/ESA_DOC/ENVISAT/MERIS/meris.ProductHandbook.2_1.pdf

European space agency. (2012). *SENTINEL-2 ESA's Optical High-Resolution Mission for GMES Operational Services*. ESA Communications.

Evans, R. H. (1999). Processing framework and match-up database (ATDB 26, v3). *Ocean Color Web Page*, 1–99. Retrieved from http://oceancolor.gsfc.nasa.gov/DOCS/atbd_mod26.pdf

FAO. (2006). *Water Monitoring - Mapping Existing Global Systems & Initiatives Background Document - August*

2006. *Water*. Stockholm. Retrieved from http://www.fao.org/docrep/010/i0213e/i0213e00.htm

Felde, G. W., Anderson, G. P., Cooley, T. W., Matthew, M. W., adler-Golden, S. M., Berk, A., & Lee, J. (2003). Analysis of Hyperion data with the FLAASH atmospheric correction algorithm. In *IGARSS 2003. 2003 IEEE International Geoscience and Remote Sensing Symposium. Proceedings (IEEE Cat. No.03CH37477)* (Vol. 1, pp. 90–92). IEEE. http://doi.org/10.1109/IGARSS.2003.1293688

Gertsch, J., Güttinger, M., Sticher, O., & Heilmann, J. (2002). Relative quantification of mRNA levels in Jurkat T cells with RT-real time-PCR (RT-rt-PCR): new possibilities for the screening of anti-inflammatory and cytotoxic compounds. *Pharmaceutical Research*, *19*(8), 1236–43. http://doi.org/10.1023/A:1019818814336

Glazer, A. N. (1989). Light guides. Directional energy transfer in a photosynthetic antenna. *The Journal of Biological Chemistry*, *264*(1), 1–4. Retrieved from http://www.ncbi.nlm.nih.gov/pubmed/2491842

Gons, H. J. (2002). A chlorophyll-retrieval algorithm for satellite imagery (Medium Resolution Imaging Spectrometer) of inland and coastal waters. *Journal of Plankton Research*, *24*(9), 947–951. http://doi.org/10.1093/plankt/24.9.947

Gons, H. J. (2004). Effect of a waveband shift on chlorophyll retrieval from MERIS imagery of inland and coastal waters. *Journal of Plankton Research*, *27*(1), 125–127. http://doi.org/10.1093/plankt/fbh151

Gons, H. J., Hakvoort, H., Peters, S. W. M., & Simis, S. G. H. (2005). Optical detection of cyanobacterial blooms: Shipboard observation and remote sensing. *Harmful Cyanobacteria*, *3*, 177–199.

Gordon, H. R., Brown, O. B., Evans, R. H., Brown, J. W., Smith, R. C., Baker, K. S., & Clark, D. K. (1988). A semianalytic radiance model of ocean color. *Journal of Geophysical Research*, *93*(D9), 10909. http://doi.org/10.1029/JD093iD09p10909

Gordon, H. R., & Franz, B. a. (2008). Remote sensing of ocean color: Assessment of the water-leaving radiance bidirectional effects on the atmospheric diffuse transmittance for SeaWiFS and MODIS intercomparisons. *Remote Sensing of Environment*, *112*(5), 2677–2685. http://doi.org/10.1016/j.rse.2007.12.010

Griffiths, B. M. (1939). Early References to Waterbloom in British Lakes. *Proceedings of the Linnean Society of London*, *151*(1), 12–19. http://doi.org/10.1111/j.1095-8312.1939.tb00189.x

Guanter, L., Ruiz-Verdú, A., Odermatt, D., Giardino, C., Simis, S., Estellés, V., … Moreno, J. (2010). Atmospheric correction of ENVISAT/MERIS data over inland waters: Validation for European lakes. *Remote Sensing of Environment*, *114*(3), 467–480. http://doi.org/10.1016/j.rse.2009.10.004

Häder, D.-P., Lebert, M., Flores-Moya, A., Jiménez, C., Mercado, J., Salles, S., … Figuero, F. L. (1997). Effects of solar radiation on the photosynthetic activity of the red alga Corallina elongata Ellis et Soland. *Journal of Photochemistry and Photobiology B: Biology*, *37*(3), 196–202. http://doi.org/10.1016/S1011-1344(96)07402-7

Hodoki, Y., Ohbayashi, K., Kobayashi, Y., Okuda, N., & Nakano, S.-I. (2011). Temporal variation in cyanobacteria species composition and photosynthetic activity in experimentally induced blooms. *Journal of Plankton Research*, *33*(9), 1410–1416. http://doi.org/10.1093/plankt/fbr040

Holland.com. (2014). Made in Holland - Water.pdf. Retrieved February 4, 2016, from http://www.hollandtradeandinvest.com/publications/publications/made-in-holland/08/7/made-in-holland---water

Huitema, D. (2002). Case Study 1 : IJsselmeer Basin, 72.

Hunter, P. D., Tyler, A. N., Carvalho, L., Codd, G. a., & Maberly, S. C. (2010). Hyperspectral remote sensing of cyanobacterial pigments as indicators for cell populations and toxins in eutrophic lakes. *Remote Sensing of Environment*, *114*(11), 2705–2718. http://doi.org/10.1016/j.rse.2010.06.006

I T T Visual Information Solutions. (2009). *Atmospheric Correction Module : QUAC and FLAASH User ' s Guide*. Retrieved from https://www.exelisvis.com/portals/0/pdfs/envi/Flaash_Module.pdf

Isenstein, E. M., Trescott, A., & Park, M.-H. (2014). Multispectral Remote Sensing of Harmful Algal Blooms in Lake Champlain, USA. *Water Environment Research*, *86*(12), 2271–2278. http://doi.org/10.2175/106143014X13975035526149

Jupp, D., Kirk, J., & Harris, G. (1994). Detection, identification and mapping of cyanobacteria — Using remote sensing to measure the optical quality of turbid inland waters. *Marine and Freshwater Research*, *45*(5), 801. http://doi.org/10.1071/MF9940801

Kanoshina, I., Lips, U., & Leppänen, J.-M. (2003). The influence of weather conditions (temperature and wind) on cyanobacterial bloom development in the Gulf of Finland (Baltic Sea). *Harmful Algae*, *2*(1), 29–41. http://doi.org/10.1016/S1568-9883(02)00085-9

Kudela, R. M., Palacios, S. L., Austerberry, D. C., Accorsi, E. K., Guild, L. S., & Torres-Perez, J. (2015). Application of hyperspectral remote sensing to cyanobacterial blooms in inland waters. *Remote Sensing of Environment*, *167*, 196–205. http://doi.org/10.1016/j.rse.2015.01.025

Kurzbaum, E., Eckert, W., & Yacobi, Y. Z. (2007). Delayed fluorescence as a direct indicator of diurnal variation in quantum and radiant energy utilization efficiencies of phytoplankton. *Photosynthetica*, *45*(4), 562–567. http://doi.org/10.1007/s11099-007-0096-z

Kutser, T. (2009). Passive optical remote sensing of cyanobacteria and other intense phytoplankton blooms in coastal and inland waters. *International Journal of Remote Sensing*, *30*(17), 4401–4425. http://doi.org/10.1080/01431160802562305

Lee, T., & Kaufman, Y. (1986). Non-Lambertian Effects on Remote Sensing of Surface Reflectance and Vegetation Index. *IEEE Transactions on Geoscience and Remote Sensing*, *GE-24*(5), 699–708. http://doi.org/10.1109/TGRS.1986.289617

Lee, Z., Carder, K. L., Hawes, S. K., Steward, R. G., Peacock, T. G., & Davis, C. O. (1994). Model for the interpretation of hyperspectral remote-sensing reflectance. *Applied Optics*, *33*(24), 5721–5732. http://doi.org/10.1364/AO.33.005721

Lorenz, N. (1999). Effects of cliamte change on the functions of the IJsselmeer area.

Lorenzoni, L., Toro-Farmer, G., Varela, R., Guzman, L., Rojas, J., Montes, E., & Muller-Karger, F. (2015). Characterization of phytoplankton variability in the Cariaco Basin using spectral absorption, taxonomic and pigment data. *Remote Sensing of Environment*, *167*, 259–268. http://doi.org/10.1016/j.rse.2015.05.002

Matthews, M. W., Bernard, S., & Robertson, L. (2012). An algorithm for detecting trophic status (chlorophyll-a), cyanobacterial-dominance, surface scums and floating vegetation in inland and coastal waters. *Remote Sensing of Environment*, *124*, 637–652. http://doi.org/10.1016/j.rse.2012.05.032

Medina-Cobo, M., Domínguez, J. A., Quesada, A., & de Hoyos, C. (2014). Estimation of cyanobacteria biovolume in water reservoirs by MERIS sensor. *Water Research*, *63*, 10–20. http://doi.org/10.1016/j.watres.2014.06.001

Mishra, S., & Mishra, D. R. (2014). A novel remote sensing algorithm to quantify phycocyanin in cyanobacterial algal blooms. *Environmental Research Letters*, *9*(11), 114003. http://doi.org/10.1088/1748-9326/9/11/114003

Mishra, S., Mishra, D. R., Lee, Z., & Tucker, C. S. (2013). Quantifying cyanobacterial phycocyanin concentration in turbid productive waters: A quasi-analytical approach. *Remote Sensing of Environment*, *133*, 141–151. http://doi.org/10.1016/j.rse.2013.02.004

Mobley, C. D. (1999). Estimation of the remote-sensing reflectance from above-surface measurements. *Applied Optics*, *38*(36), 7442–55. Retrieved from http://www.ncbi.nlm.nih.gov/pubmed/18324298

Mueller, J. L., Fargion, G. S., McClain, C. R., Pegau, S., Zaneveld, J. R. V., Mitchell, B. G., … Stramska, M. (2003). Ocean Optics Protocols for Satellite Ocean Color Sensor Validation. Volume 4; Inherent Optical Properties: Instruments, Characterizations, Field Measurements and Data Analysis

Protocols; Revised. Retrieved from http://ntrs.nasa.gov/search.jsp?R=20030065253

Ogashawara, I., Mishra, D. R., Mishra, S., Curtarelli, M. P., & Stech, J. L. (2013). A performance review of reflectance based algorithms for predicting phycocyanin concentrations in inland waters. *Remote Sensing*, *5*(10), 4774–4798. http://doi.org/10.3390/rs5104774

Palmer, S. C. J., Hunter, P. D., Lankester, T., Hubbard, S., Spyrakos, E., N. Tyler, A., … Tóth, V. R. (2015). Validation of Envisat MERIS algorithms for chlorophyll retrieval in a large, turbid and optically-complex shallow lake. *Remote Sensing of Environment*, *157*, 158–169. http://doi.org/10.1016/j.rse.2014.07.024

Paul, M. J. (2001). Sink regulation of photosynthesis. *Journal of Experimental Botany*, *52*(360), 1383–1400. http://doi.org/10.1093/jexbot/52.360.1383

Reinart, A., & Kutser, T. (2006). Comparison of different satellite sensors in detecting cyanobacterial bloom events in the Baltic Sea. *Remote Sensing of Environment*, *102*(1-2), 74–85. http://doi.org/10.1016/j.rse.2006.02.013

Richardson, L. L. (1996). Remote Sensing of Algal Bloom Dynamics. *BioScience*, *46*(7), 492–501. http://doi.org/10.2307/1312927

Ruiz-Verdú, A., Simis, S. G. H., de Hoyos, C., Gons, H. J., & Peña-Martínez, R. (2007). An evaluation of algorithms for the remote sensing of cyanobacterial biomass. *Remote Sensing of Environment*, *112*(11), 3996–4008. http://doi.org/10.1016/j.rse.2007.11.019

Salama, M. S., Van Der Velde, R., Van Der Woerd, H. J., Kromkamp, J. C., Philippart, C. J. M., Joseph, a. T., … Su, Z. (2012). *Technical Note: Calibration and validation of geophysical observation models*. *Biogeosciences* (Vol. 9).

Santamaria-del-Angel, E., Millan-Nunez, R., Gonzalez-Silvera, A., & Cajal-Medrano, R. (2011). Comparison of In Situ and Remotely-Sensed Chl-a Concentrations: A Statistical Examination of the Match-up Approach. *Handbook of Satellite Remote Sensing Image Interpretation: Marine Applications*, 293.

Simis, S. G. H. (2006). *Blue - green catastrophe: remote sensing of mass viral lysis of cyanobacteria*. Vrije Universiteit Amsterdam. Retrieved from http://dare.ubvu.vu.nl/bitstream/handle/1871/10641/7574.pdf?sequence=1

Simis, S. G. H., Peters, S. W. M., & Gons, H. J. (2005). Remote sensing of the cyanobacterial pigment phycocyanin in turbid inland water. *Limnology and Oceanography*, *50*(1), 237–245. http://doi.org/10.4319/lo.2005.50.1.0237

SUHET. (2015). *SENTINEL-2UserHandbook SENTINEL-2 User Handbook*. Retrieved from https://sentinel.esa.int/documents/247904/685211/Sentinel-2_User_Handbook

Sun, D., Hu, C., Qiu, Z., & Shi, K. (2015). Estimating phycocyanin pigment concentration in productive inland waters using Landsat measurements: A case study in Lake Dianchi. *Optics Express*, *23*(3), 3055. http://doi.org/10.1364/OE.23.003055

The Columbia Encyclopedia, 6th ed. (2015). IJsselmeer Facts, information, pictures | Encyclopedia.com articles about IJsselmeer. Retrieved February 3, 2016, from http://www.encyclopedia.com/topic/IJsselmeer.aspx

TheIJsselmeer.com. (2016). IJsselmeer | vacationhouses, apartments and chalets in North Holland, vacation at the water. Retrieved February 4, 2016, from http://theijsselmeer.com/

UNEP. (2009). *The Wadden Sea , Germany and Netherlands (N1314) - Extension Denmark and Germany*. Wilhelmshaven. Retrieved from http://www.waddensea-secretariat.org/sites/default/files/downloads/volume_i_-_the_wadden_sea_germany_and_netherlands_n1314_lq.pdf

USGS. (2013). Turbidity -- Units of Measurement. Retrieved October 12, 2015, from http://or.water.usgs.gov/grapher/fnu.html

usgs. (2013). Using the USGS Landsat 8 Product. Retrieved August 5, 2015, from http://landsat.usgs.gov/Landsat8_Using_Product.php

USGS. (2015). *Landsat 8 (L8) Data Users Handbook Version 1.0 June 2015*. Sioux Falls, South Dakota. Retrieved from http://landsat.usgs.gov/documents/Landsat8DataUsersHandbook.pdf

Vincent. (2009). Cyanobacteria. *Protists, Bacteria and Fungi: Planktonic and Attached*, 226–232. Retrieved from http://www.cen.ulaval.ca/warwickvincent/PDFfiles/228.pdf

Vincent, R. K., Qin, X., McKay, R. M. L., Miner, J., Czajkowski, K., Savino, J., & Bridgeman, T. (2004). Phycocyanin detection from LANDSAT TM data for mapping cyanobacterial blooms in Lake Erie. *Remote Sensing of Environment*, *89*(3), 381–392. http://doi.org/10.1016/j.rse.2003.10.014

Water insight. (2015). *WISP-3 User Guide. Handbook* (Version 1.). Wageningen: Water Insight BV. Retrieved from http://www.waterinsight.nl/sites/www.waterinsight.nl/files/Manual WISP_dec 2010.pdf

Wheeler, S. M., Morrissey, L. A., Levine, S. N., Livingston, G. P., & Vincent, W. F. (2012). Mapping cyanobacterial blooms in Lake Champlain's Missisquoi Bay using QuickBird and MERIS satellite data. *Journal of Great Lakes Research*, *38*, 68–75. http://doi.org/10.1016/j.jglr.2011.06.009

windfinder. (2016). Wind & weather statistics Enkhuizen - Windfinder. Retrieved March 14, 2016, from http://www.windfinder.com/windstatistics/enkhuizen

Wynne, T. T., Stumpf, R. P., & Richardson, A. G. (2006). Discerning resuspended chlorophyll concentrations from ocean color satellite imagery. *Continental Shelf Research*, *26*(20), 2583–2597. http://doi.org/10.1016/j.csr.2006.08.003

Zheng Zhou, Yuanling Zhao, & Dengke Fan. (2011). Research on cyanobacteria blooms monitoring ability of HJ-1 CCD. In *2011 International Conference on Image Analysis and Signal Processing* (pp. 546–549). IEEE. http://doi.org/10.1109/IASP.2011.6109103

APPENDIX 1

Band ratios 1. Landsat 8 OLI
2. Sentinel-2 MSI

a. Bands needed for the Calculation of Band ratios for Landsat 8 OLI.

Landsat 8 OLI	**Bands**	**Band 1**	**Band 2**	**Band 3**	**Band 4**	**Band 5**
	Becomes		**Band 1**	**Band 2**	**Band 3**	**Band 4**
	Band No.	**443 (nm)**	**489 (nm)**	**561 (nm)**	**658 (nm)**	**864.5 (nm)**
	Site 1	0.017508	0.025311	0.0429	0.026064	0.015
	Site 2	0.0135	0.022711	0.0441	0.024327	0.014667
	Site 3	0.0169	0.029133	0.050997	0.028727	0.017234
	Site 4	0.0137	0.025833	0.0582	0.028127	0.0157
	Site 5	0.019008	0.031733	0.0641	0.034691	0.021567
	Site 6	0.003188	0.011246	0.028827	0.011075	0.002084
	Site 7	0.005751	0.014652	0.035409	0.015528	0.008356
	Site 8	0.005239	0.01323	0.031912	0.01482	0.006414
	Site 9	0.001054	0.01081	0.032597	0.010675	0.000887
	Site 10	0.001999	0.012051	0.0337	0.01225	0.002272
	Site 11	0.006114	0.016695	0.040054	0.017929	0.009971
	Site 12	-0.00292	0.008387	0.036472	0.01007	-0.00127
	Site 13	-0.00075	0.011185	0.039757	0.012212	0.000745
	Site 14	0.002713	0.012802	0.039371	0.014178	0.002705
	Site 15	0.004496	0.011726	0.030189	0.012031	0.003744
	Site 16	0.005733	0.016504	0.045179	0.018718	0.004736
	Site 17	0.005733	0.016504	0.045179	0.018718	0.004736
	Site 18	0.003696	0.013481	0.038356	0.015415	0.003611
	Site 19	0.004021	0.014146	0.040408	0.016045	0.003678
	Site 20	0.003621	0.012573	0.035396	0.012878	0.002027

b. Bands needed for Sentinel-2 MSI band ratio

Sentinel-2 MSI	**Bands**	**Band 1**	**Band 2**	**Band 3**	**Band 4**	**Band 5**
		443 (nm)	**490 (nm)**	**560 (nm)**	**665 (nm)**	**865 (nm)**
	Site 1	0.017508	0.025789	0.042709	0.023	0.015
	Site 2	0.0135	0.023194	0.044	0.021164	0.014667
	Site 3	0.0169	0.029989	0.0508	0.024964	0.017234
	Site 4	0.0137	0.026689	0.058291	0.023964	0.0157
	Site 5	0.019008	0.032683	0.064	0.030264	0.021567
	Site 6	0.003188	0.011604	0.028715	0.009185	0.002084
	Site 7	0.005751	0.015128	0.035368	0.013538	0.008356
	Site 8	0.005239	0.013616	0.031747	0.012821	0.006414
	Site 9	0.001054	0.011331	0.032533	0.008481	0.000887

	Site 10	0.001999	0.012614	0.033532	0.010036	0.002272
	Site 11	0.006114	0.017291	0.039978	0.015809	0.009971
	Site 12	-0.00292	0.008963	0.036433	0.007385	-0.00127
	Site 13	-0.00075	0.011912	0.03967	0.00943	0.000745
	Site 14	0.002713	0.013332	0.039243	0.01134	0.002705
	Site 15	0.004496	0.012059	0.0301	0.010285	0.003744
	Site 16	0.005733	0.01699	0.045035	0.015971	0.004736
	Site 17	0.005733	0.01699	0.045035	0.015971	0.004736
	Site 18	0.003696	0.013882	0.03821	0.013071	0.003611
	Site 19	0.004021	0.014571	0.040255	0.013556	0.003678
	Site 20	0.003621	0.012958	0.035295	0.010665	0.002027

c. Derived band ratios for Landsat 8 OLI.

	Ratio 1	Ratio 2	Ratio 3	Ratio 4	Ratio 43	Ratio 42	Ratio 41	Ratio 32	Ratio 31	Ratio 21
Band No.	489.000	561.000	658.000	864.500						
Site 1	0.018	0.025	0.043	0.026	0.608	1.030	1.489	1.695	2.450	1.446
Site 2	0.014	0.023	0.044	0.024	0.552	1.071	1.802	1.942	3.267	1.682
Site 3	0.017	0.029	0.051	0.029	0.563	0.986	1.700	1.750	3.018	1.724
Site 4	0.014	0.026	0.058	0.028	0.483	1.089	2.053	2.253	4.248	1.886
Site 5	0.019	0.032	0.064	0.035	0.541	1.093	1.825	2.020	3.372	1.669
Site 6	0.003	0.011	0.029	0.011	0.384	0.985	3.474	2.563	9.041	3.527
Site 7	0.006	0.015	0.035	0.016	0.439	1.060	2.700	2.417	6.157	2.548
Site 8	0.005	0.013	0.032	0.015	0.464	1.120	2.829	2.412	6.092	2.525
Site 9	0.001	0.011	0.033	0.011	0.327	0.987	10.128	3.015	30.927	10.257
Site 10	0.002	0.012	0.034	0.012	0.364	1.016	6.128	2.796	16.857	6.028
Site 11	0.006	0.017	0.040	0.018	0.448	1.074	2.932	2.399	6.552	2.731
Site 12	-0.003	0.008	0.036	0.010	0.276	1.201	-3.446	4.348	-12.479	-2.870
Site 13	-0.001	0.011	0.040	0.012	0.307	1.092	-16.223	3.554	-52.816	-14.860
Site 14	0.003	0.013	0.039	0.014	0.360	1.108	5.226	3.075	14.511	4.718
Site 15	0.004	0.012	0.030	0.012	0.399	1.026	2.676	2.575	6.715	2.608
Site 16	0.006	0.017	0.045	0.019	0.414	1.134	3.265	2.738	7.880	2.879
Site 17	0.006	0.017	0.045	0.019	0.414	1.134	3.265	2.738	7.880	2.879
Site 18	0.004	0.013	0.038	0.015	0.402	1.144	4.171	2.845	10.379	3.648
Site 19	0.004	0.014	0.040	0.016	0.397	1.134	3.991	2.856	10.050	3.518
Site 20	0.004	0.013	0.035	0.013	0.364	1.024	3.557	2.815	9.776	3.472

d. Derived band ratios for Sentinel-2 MSI.

	1	2	3	4	5	6	7	8	9	10
Bands	**Ratio 1**	**Ratio 2**	**Ratio 3**	**Ratio 4**	**Ratio 43**	**Ratio 42**	**Ratio 41**	**Ratio 32**	**Ratio 31**	**Ratio 21**
Band No.	**490**	**560**	**667**	**865**						
Site 1	0.017508	0.025789	0.042709	0.015	0.032141	0.581653	0.856735	1.656105	2.439328	1.472931
Site 2	0.0135	0.023194	0.044	0.014667	0.032641	0.632358	1.086451	1.897019	3.259259	1.718095
Site 3	0.0169	0.029989	0.0508	0.017234	0.0364	0.574691	1.019773	1.693979	3.005917	1.774472
Site 4	0.0137	0.026689	0.058291	0.0157	0.041641	0.588267	1.145985	2.184134	4.254849	1.948071
Site 5	0.019008	0.032683	0.064	0.021567	0.049081	0.65989	1.134612	1.958213	3.366944	1.719396
Site 6	0.003188	0.011604	0.028715	0.002084	0.012507	0.179559	0.653522	2.474547	9.006363	3.6396
Site 7	0.005751	0.015128	0.035368	0.008356	0.017512	0.552339	1.452898	2.337911	6.149754	2.630449
Site 8	0.005239	0.013616	0.031747	0.006414	0.016631	0.47107	1.224365	2.331592	6.060073	2.599114
Site 9	0.001054	0.011331	0.032533	0.000887	0.01191	0.078326	0.84203	2.871293	30.86746	10.75037
Site 10	0.001999	0.012614	0.033532	0.002272	0.013342	0.180086	1.136302	2.658267	16.77304	6.309763
Site 11	0.006114	0.017291	0.039978	0.009971	0.019388	0.576696	1.630977	2.312143	6.539062	2.82814
Site 12	-0.00292	0.008963	0.036433	-0.00127	0.013089	-0.14151	0.433958	4.064957	-12.4657	-3.06663
Site 13	-0.00075	0.011912	0.03967	0.000745	0.015208	0.062583	-0.99036	3.330261	-52.7004	-15.8247
Site 14	0.002713	0.013332	0.039243	0.002705	0.017933	0.202898	0.996975	2.943575	14.46379	4.91368
Site 15	0.004496	0.012059	0.0301	0.003744	0.012989	0.310475	0.83284	2.496001	6.695456	2.682473
Site 16	0.005733	0.01699	0.045035	0.004736	0.021186	0.278736	0.826032	2.650647	7.855168	2.963491
Site 17	0.005733	0.01699	0.045035	0.004736	0.021186	0.278736	0.826032	2.650647	7.855168	2.963491
Site 18	0.003696	0.013882	0.03821	0.003611	0.017178	0.260134	0.977146	2.752551	10.33946	3.756318
Site 19	0.004021	0.014571	0.040255	0.003678	0.017871	0.25241	0.914705	2.762768	10.01196	3.623888
Site 20	0.003621	0.012958	0.035295	0.002027	0.00241	0.156403	0.559767	2.723672	9.748008	3.578995

APPENDIX 2

A. PC correlation between the bands and band ratios for Sun Model.

	blue	Green	red	NIR	Nearred	Near green	Nearblue	redgreen	redblue	greenblue	PC
blue	1										
Green	0.972733	1									
red	0.745376	0.8662	1								
NIR	0.954055	0.991535	0.905324	1							
Nearred	0.95399	0.882727	0.571887	0.861191	1						
Near green	-0.24476	-0.15254	0.199056	-0.03424	-0.23307	1					
Nearblue	0.120125	0.03234	-0.12342	0.013109	0.152564	-0.278	1				
redgreen	-0.87239	-0.77269	-0.41365	-0.72896	-0.92384	0.488375	-0.33074	1			
redblue	0.10874	0.021086	-0.13285	0.000378	0.136925	-0.28911	0.999542	-0.31759	1		
greenblue	0.103604	0.016543	-0.14261	-0.00672	0.131964	-0.30709	0.998564	-0.31464	0.999353	1	
PC	0.018346	-0.02449	-0.09493	-0.03055	0.056355	0.07228	-0.5105	0.066455	-0.50914	-0.51162	1

B. PC correlation between bands and bands ratios for Vincent model.

	B3/B1	B4/B1	B4/B3	B5/B3	PC
B3/B1	1				
B4/B1	0.895064	1			
B4/B3	-0.84892	-0.53105	1		
B5/B3	-0.92587	-0.76081	0.86955	1	
PC	-0.03868	0.032819	0.161593	0.073545	1